Chapter 2
Climate Variability and Climate Change: Past and Future

Xuejie Gao, Qingyun Duan, Tinghai Ou, Yuanhai Fu, Xuewei Fan, Zhu Liu, Chiyuan Miao, and Chenwei Shen

Abstract The LMRB (LMRB) has experienced significant climate change, particularly over the last 50 years. An increase in the annual precipitation but with significant seasonal differences in the changes, and a remarkable warming are observed over the Basin. The region also experienced more frequent extreme events, such as an increase in extreme precipitation, as well as hot days and warm nights, a decrease in cold days and cold nights, and a more frequent occurrence of droughts. The future climate over

X. Gao (✉) · Y. Fu
Climate Change Research Center, Institute of Atmospheric Physics, Chinese Academy of Sciences, No. 81 Beichen West Road, Chaoyang District, Beijing, China
e-mail: gaoxuejie@mail.iap.ac.cn

Y. Fu
e-mail: fugreen1981@mail.iap.ac.cn

Q. Duan · Z. Liu
College of Hydrology and Water Resources, Hohai University, 1 Xikang Road, Nanjing, Jiangsu, China
e-mail: qyduan@hhu.edu.cn

Z. Liu
e-mail: zhuliu@hhu.edu.cn

T. Ou
Department of Earth Sciences, University of Gothenburg, Medicinaregatan 7B, Gothenburg, Sweden
e-mail: tinghai.ou@gu.se

X. Fan · C. Miao
Faculty of Geographical Science, Beijing Normal University, No. 19 Xinjiekouwai Street, Haidian District, Beijing, China
e-mail: 201831051005@bun.edu.cn

C. Miao
e-mail: miaocy@bnu.edu.cn

C. Shen
High Performance Computing Department, Sugon Corporation, No. 36, Zhongguancun Software Park, Haidian District, Beijing, China
e-mail: shenchw@sugon.com

D. Chen et al. (eds.), *Water Resources in the Lancang-Mekong River Basin: Impact of Climate Change and Human Interventions*,
https://doi.org/10.1007/978-981-97-0759-1_2

the Basin is projected to be continuous warming, which is most significant by the end of the twenty-first century. A general wetting is projected over the region with the spatial pattern of the projected annual total precipitation change show consistencies with the present day condition. Differences are found between the global and regional climate model projections in the precipitation, indicating the uncertainties existing in the projections, and also the importance of the model resolution in projecting future climate.

2.1 Introduction

The region encompassing the Lancang-Mekong River has a plateau climate in its source region, but a typical monsoonal climate in most of the basin, with the monsoons often accompanied by the extreme events of heatwaves, droughts and floods, and tropical cyclones, (e.g. Chang et al., 2012; Ding & Chan, 2005; Tanggang et al., 2007). Many studies have shown that significant climate change has been observed over the region during the last century, particularly over the last 50 years. Since the middle of the twentieth century, the average surface temperature and heat wave frequency have increased for the region. During 1952–2015, the annual precipitation trend was 0.5 mm/10 yr. However, there exists a significant difference between the dry and wet season. On the basin scale, a significant ($p < 0.05$) trend of wetting by 3.4 mm/10 yr was found in the dry season during water years 1952–2015, whereas in the wet season, there was a drying trend of −3.0 mm/10 yr (Irannezhad et al., 2020). The temperature in the LMRB has risen at a rate of 0.76 °C/10 yr during 1980–2010 (Fan & He, 2015). Extreme temperature events show also an upward trend (Thirumalai et al., 2017) with an increase in hot days and warm nights, and a decrease in cold days and cold nights (Ma et al., 2013).

Observations and model-based analysis form an important basis for gaining a scientific understanding of the climate variability and change that have occurred in the past, what are occurring right now, and what are going to happen in the future. Unfortunately, this region has a relatively sparse climate observational network. In climate studies, global datasets like the Global Precipitation Climatology Centre (GPCC) data (Adler et al., 2017) and gridded precipitation and other meteorological variables developed by the Climate Research Unit (CRU) of the University of Anglia (Harris et al., 2013) have often been used to investigate the observed climate change in the LMRB (Fan & He, 2015; Irannezhad et al., 2020). The dataset of Asian Precipitation-Highly Resolved Observational Data Integration Toward Evaluation of water resources (APHRODITE), generated by the Research Institute for Humanity and Nature and the Meteorological Research Institute of the Japan Meteorological Agency, is a long term regional daily-scale gridded precipitation dataset, generated by utilizing a dense network of in situ gauge records in Asia and, therefore, is better suited for climate studies in the LMRB (Irannezhad et al., 2020; Yatagai et al., 2009).

It is necessary to resort to climate models to gain insights into future climate change. As the primary tools in climate change studies, global climate models

(GCMs) have been widely used to simulate and project climate change at the global scale. The Intergovernmental Panel on Climate Change (IPCC) gathers and evaluates GCMs as part of the international climate change Assessment Reports (AR). IPCC has so far published six Assessment Reports (ARs). In each AR, the IPCC relies on the outputs of the GCMs participating in the Climate Model Intercomparison Projects (CMIPs). Archives of GCM outputs from different CMIPs offer opportunities to assess the climate model performance in simulating past climate and to analyse the projections for 21st-century climate change under different emission scenarios, and the potential effects of the changes at either global or regional scales (Bannister et al., 2017; Su et al., 2013).

The current phase of CMIP is the sixth (CMIP6). The GCMs in CMIP6 have significant improvements in the physical parameterisations (e.g. in representing the clouds), spatial resolution, and inclusion of additional Earth system components (e.g. ice sheets) and processes (e.g. the nutrient limitations in terrestrial carbon cycle), compared to those of the previous CMIPs (Eyring et al., 2016, 2019). In CMIP6, a new conceptual framework had been developed. It uses a diverse range of socioeconomic and technological development scenarios, i.e. the Shared Socioeconomic Pathways (SSPs). SSPs are distinguished on the basis of anticipated challenges to adaptation and mitigation, which is different from the emissions pathways concluded in the IPCC Special Report on Emissions Pathways/Scenarios (Moss et al., 2010; O'Neill et al., 2016). The two main axes of the scenario matrix architecture are firstly, the future climate radiative forcing level which is characterized by the Representative Concentration Pathways (RCPs), and secondly, a set of alternative plausible trajectories for future global development (the SSPs) (Kriegler et al., 2014). The SSPs are based on five narratives describing the alternative pathways of socioeconomic development, including SSP1 for sustainable development, SSP2 for middle-of-the-road development, SSP3 for regional rivalry, SSP4 for inequality, and SSP5 for fossil-fueled development (Calvin et al., 2017; Fricko et al., 2017; Fujimori et al., 2017; Kriegler et al., 2017; van Vuuren et al., 2017). This new generation of pathways/scenarios will facilitate the understanding of plausible socioeconomic and climate futures for the society.

While GCMs have contributed greatly to our understanding of climate variability and climate change at the global scale, they generally have rough spatial resolution and cannot capture the spatial climate change features at regional scales. To understand climate change at regional and local scales, one can use high-resolution regional climate models (RCMs), which are the limited area climate models forced by specified lateral conditions from GCMs or reanalysis. RCMs simulate atmospheric and land surface conditions, including Greenhouse Gas (GHG) and aerosol forcings. RCMs apply a dynamic downscaling approach to fill the gap between the coarse estimates of GCMs, which have practical requirements in the regional and locale scale impact studies, e.g. the finer spatial distribution of precipitation needed in hydrologic operations over small basins under global warming. RCMs have provided data for the impact studies and policymakers since the last three decades, and helped to increase knowledge of the present-day climate and future changes at regional levels,

thus making them an important tool for investigating climate change in the LMRB (Tapiador et al., 2020).

This chapter describes the space–time features of climate variability and climate change over the LMRB based on climate observations and the GCM outputs from CMIP6 and the RCM outputs that are driven by GCMs from CMIP5. It is organized as follows. In Sect. 2.2, the climate change that has occurred in the LMRB over the last century is examined based on climate observations. Section 2.3 presents the simulations of the past climate and projections of future climate changes based on simulation and projection results from RCMs. In Sect. 2.4, a multi-model analysis of climate change in the LMRB is presented using the latest GCM outputs from CMIP6.

2.2 Past Climate Change from Observations and Simulations

There are a few rain gauges and stations with both temperature and precipitation records available over the LMRB (e.g., Wang et al., 2016). The data quality, in terms of continuity, is also quite low. Only very few stations have high quality data covering the latest 20-year period of model historical simulation, i.e., 1995–2014. Most of the stations with high quality data are located above the LMRB. To analyse the long-term (1961–2015) spatial–temporal variation of temperature and precipitation over the whole LMRB, gridded data sets interpolated from station data have been used in this work. For this purpose, gridded near-surface air temperature (T2m) and daily precipitation from the APHRODITE (http://aphrodite.st.hirosaki-u.ac.jp/index.html) during 1961–2015 are adopted (Yasutomi et al., 2011; 2012). The horizontal resolution of the APHRODITE data sets is 0.25° × 0.25° (latitude × longitude). Annual mean T2m and total precipitation are calculated based on the daily data sets. The average during 1961–2015 and 1995–2014 is to be shown together with their difference to illustrate the climate change during the recent 20 years which has been used for model evaluation. Empirical Orthogonal Function (EOF) analysis is also performed to show the major spatial–temporal variation patterns over the LMRB during 1961–2015.

Four extreme indices are investigated to illustrate the changes in extremes over the LMRB (Table 2.1). The two precipitation extreme indices (Rx5day and CDD) are calculated based on the gridded daily precipitation and temperature from the APHRODITE. Since there are no maximum and minimum temperatures available in APHRODITE, the two temperature extreme indices (TXx and TNn) from HadEX 3.0.3 (Dunn et al., 2020) are adopted. The HadEX data, with horizontal resolution 1.25° × 1.875° (latitude × longitude), have been interpolated to the APHRODITE data grid covering the LMRB using the inverse distance weighting (power 2) interpolation method.

Table 2.1 Definitions of the extreme temperature indices used

Index	Definition	Units
Rx5day	Annual maximum consecutive 5-day precipitation	mm
CDD	Annual maximum length of dry spell: maximum number of consecutive days with RR < 1 mm	Days
TXx	Annual maximum value of daily maximum temperature	°C
TNn	Annual minimum value of daily minimum temperature	°C

2.2.1 Near-Surface Air Temperature Change and Variability

The spatial variations in the annual mean T2m are quite large over the LMRB. The annual mean T2m increases from the northern to the southern river Basin, with the annual mean T2m lower than 0 °C over the northernmost of the headwater region and close to 30.0 °C over the southern Mekong Delta (Fig. 2.1a).

The annual mean T2m has significantly increased since 1950 when averaged over the whole Basin (Liu & Wang, 2020), which is higher than the mean global warming rate (Liu et al., 2021). Except for the southern Tonle Sap region, there is an overall significant warming trend over the LMRB. (Fig. 2.1b). The spatial pattern of the annual mean T2m during the recent 20 years, i.e. during 1995–2014, is similar to that during 1961–2015 but with an overall warm anomaly (Fig. 2.1c). The anomaly pattern of 1995–2014 with reference to 1961–2015 is similar to the linear trend of the annual mean T2m during 1961–2015 (Fig. 2.1d).

There are also regional and seasonal differences in the warming trend over the LMRB. For example, the warming is obvious during May and August compared to other months when averaging the whole basin (Liu & Wang, 2020), while winter T2m rise does the largest contribution to the annual T2m increase over the upper Lancang River (Wang et al., 2020). There is also obvious inter-decadal variation in the annual mean T2m. Even though there has been a general warming during the

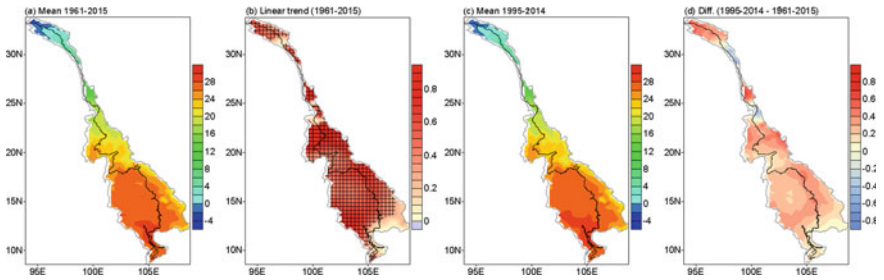

Fig. 2.1 Spatial distribution of **a** annual mean 2-m air temperature (T2m; °C) and its linear trend (°C/10 yr) during 1961–2015 (**b**), **c** annual mean T2m during 1995–2014 (°C), **d** the difference between mean T2m during 1995–2014 and 1961–2015 (°C) based on daily T2m from the APHRODITE (Yasutomi et al., 2011) (Areas with crosses show the region where the trend is significant at 0.05 level)

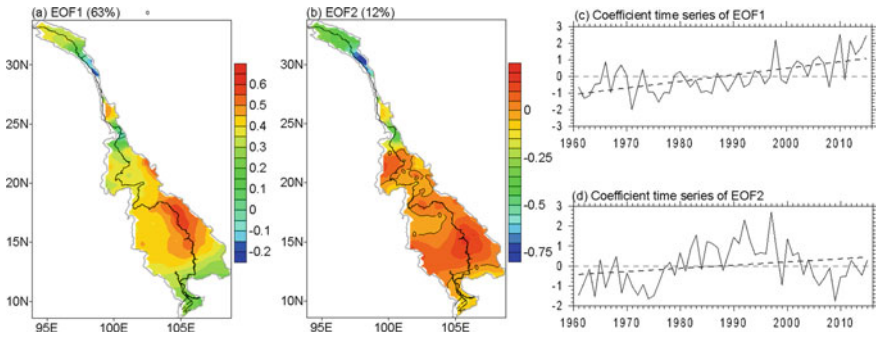

Fig. 2.2 Spatial distribution of **a** EOF1 and **b** EOF2 (°C) of annual mean T2m, and the coefficient time series of EOF1 (**c**) and EOF2 (**d**) during 1961–2015 based on daily T2m from the APHRODITE

past 60 years, there is a decrease in the annual T2m over some areas, especially over the middle and lower reaches of the Basin after 2008 (Liu & Wang, 2020). Wu et al. (2011) also show a decreasing trend in the annual T2m of Vientiane, Chaiyaphum, and Ho Chi Minh stations during 1980–2009, especially after around 2000.

The spatial variation in the warming trend is well illustrated in the first two EOF patterns, which explain 75% of the total variance of annual mean T2m (Fig. 2.2). Overall, there is a significant increase in the annual mean T2m over most of the Basin as shown in EOF1 and the related coefficient time series. There is also a change in the coefficient time series of EOF2 around 2000, centered over the middle and lower reaches of the Basin. This is related to the above-mentioned temperature decrease over these regions. The explained covariance of EOF1 is 63%, while it is only 12% for EOF2 (Fig. 2.2). The warming trend shown in Fig. 2.1b is largely explained by the EOF1 with a linear increase (Fig. 2.2c). Besides, there is a linear increase in the time series of EOF2 during the whole period which emphasize the warming covering a large part of the study area (Fig. 2.2d). Combining the first two EOFs, the warming is large over the middle to lower reaches of the river basin, with less warming over the southeast area.

In general, both GCMs and RCMs are more accurate in space than time (Huang et al., 2014; Sun et al., 2020), with a good ability to simulate the spatial distribution pattern of temperature. Models tend to underestimate the annual mean temperature in the upper and lower reaches of the Mekong River Basin, with a larger cold bias in the cold season than in the warm season (Ruan et al., 2019). Models can capture the warming characteristics in the basin, but the accuracy of the simulation is not good enough (Huang et al., 2014).

2.2.2 *Precipitation Change and Variability*

The climate of the LMRB belongs to the tropical monsoon (MRC, 2010). About 80–90% of the annual total precipitation falls from May to October (Costa-Cabral et al., 2008). The precipitation over the region is affected by Indian summer monsoon, East Asian summer monsoon, South Asian Summer Monsoon, as well as El Niño-Southern Oscillation (ENSO) (Dang et al., 2020; Fan & Luo, 2019; Hasson et al., 2013; Irannezhad et al., 2020; Räsänen & Kummu, 2013; Wang et al., 2022; Yang et al., 2019). Tropical Cyclones also have large effects on the total precipitation, especially in the southwest Basin (Chen et al., 2019), where GCMs have shown reliable skill in realistically simulating the track densities of Tropical Cyclones (Chen et al., 2020a, 2020b). On average, the northern headwater region is relatively dry with annual total precipitation of around 500 mm, while the southeastern region is relatively wet with annual total precipitation of more than 2000 mm (Fig. 2.3a).

Changes in annual precipitation are small during the period 1951–2017 when averaged over the whole Basin (Liu & Wang, 2020). A large spatial–temporal variation is obvious in the changes in precipitation. There is a decreasing trend in June and August and a small increasing trend in other months during 1951–2017 (Liu & Wang, 2020). Fan and He (2015) also show an increase in spring precipitation. Spatially, annual precipitation has slightly increased during 1960–2009 over the upper reach of the Mekong River, while a significantly decreasing trend has been found since 2000 (Wu et al., 2016). There are significant wetting and drying trends in annual total precipitation over the northeastern and most westerly parts of the Mekong River Basin during 1952–2015 (Irannezhad et al., 2020). A similar spatial pattern of the trend in annual precipitation can be found during 1961–2005 (Fig. 2.3b). In general, the rainy season precipitation contributes a large part to the annual total precipitation over the Basin (Chen et al., 2018). The spatial pattern of the interannual variability in the rainy season precipitation is highly correlated with the Indian monsoon and Western North Pacific monsoon co-variability (Yang et al., 2019). Asian monsoon circulation has weakened since the end of the 1970s due to the rapid warming in the Indian Ocean (Sooraj et al., 2015), which leads to a reduction of monsoon precipitation over the Basin. The less frequent tropical cyclones (Chen et al., 2019) may also

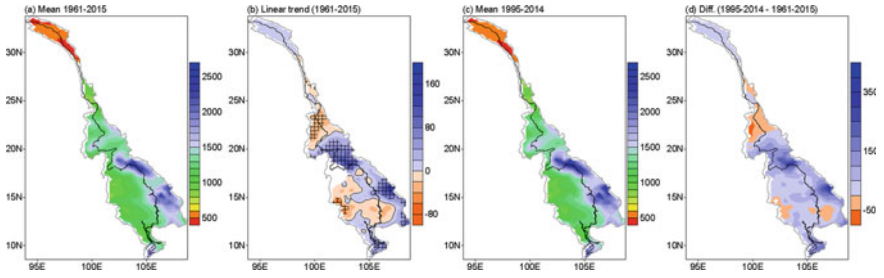

Fig. 2.3 Same as Fig. 2.1, but for annual total precipitation (Precip; mm) from the APHRODITE

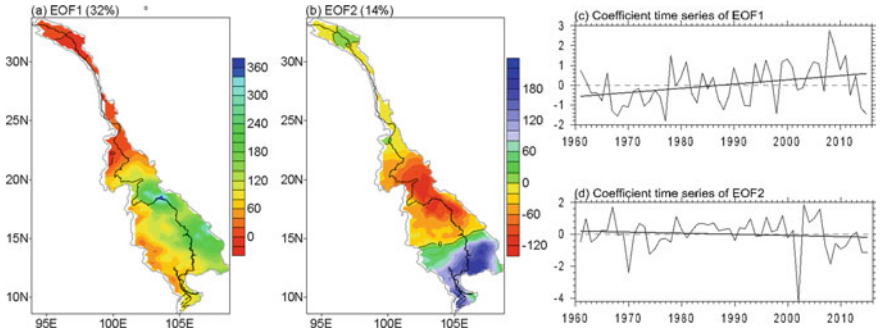

Fig. 2.4 Same as Fig. 2.2, but for annual total precipitation from the APHRODITE

lead to a decrease in wet-season precipitation over the region. The regional increase in precipitation can be attributed to the increase in extreme precipitations as shown by Li et al. (2022).

The spatial pattern of the annual precipitation during 1995–2014 is similar to that during 1961–2015 but with an overall wet difference (Fig. 2.3c). The difference pattern between 1995–2014 and 1961–2015 is similar to the linear trend of the annual precipitation during 1961–2015 (Fig. 2.3d).

The spatial–temporal variations of the annual precipitation over the River Basin can be clearly seen in the two EOF patterns and the related coefficient time series (Fig. 2.4). As can be seen in the first EOF pattern and the related coefficient time series, there is a general increase in the annual precipitation for the whole basin before 2009, while a decreasing trend is obvious afterwards. There is also a clear inter-annual dipole variation in the annual precipitation between the south and middle to the north Basin as can be seen from the second EOF pattern.

The observed spatial pattern and seasonal variation of the mean precipitation are well captured by GCMs (Ruan et al., 2018; Wang et al., 2017). A large part of GCMs evaluated have overestimated precipitation over the River Basin, especially during the monsoon season (Hasson et al., 2016; Ruan et al., 2018). Ruan et al. (2018) also pointed out that GCMs have a general failure in capturing observed trends in the wet season (53% of GCMs failed) and the dry season (65% of GCMs failed), as well as for annual total precipitation (44% of GCMs failed) over the lower Mekong Basin.

2.2.3 Variations and Changes in Weather and Climate Extreme Events

The LMRB is affected by increasing frequency both in extreme precipitation and drought, especially over the lower Mekong Basin (Liu et al., 2020; Tian et al., 2020). Extreme precipitation has generally decreased in the upper Mekong Basin but increased in the lower Mekong Basin during 1951–2015 (Irannezhad et al., 2021;

Liu et al., 2020). As can be seen from Fig. 2.5, the maximum extreme precipitation, maximum consecutive 5-day precipitation (Rx5day), is located over the east of the lower Mekong Basin. There are some regions with a significant increasing or decreasing trend in Rx5day over the lower or middle Mekong Basin respectively. The spatial pattern of mean Rx5day during 1961–2015 is similar to that of 1995–2014, with the anomaly pattern of 1995–2014 to 1961–2015 similar to the linear trend during 1961–2015. There is a general increase and decrease in the spatial–temporal variations of Rx5day over the upper/lower and middle Mekong Basin respectively as shown in Fig. 2.6.

There is a high agreement in the trend of drought frequency over the lower Mekong Basin. Adamson and Bird (2010) point out that Thailand, Cambodia, Laos, and Vietnam over the lower Mekong Basin, are vulnerable to increasing droughts. Guo et al. (2017) found an increasing trend in the frequency of drought over the north and south parts of the lower Mekong Basin during 1981–2016, with the Mekong Delta tending to have more long-term and extreme drought events. Lee and Dang (2019) also show that even though there is a decrease in the frequency of drought over the Mekong Delta during 1984–2015, there was a tendency to increase in the spatial distribution of drought with moderate and severe droughts over the region. Tian et al.

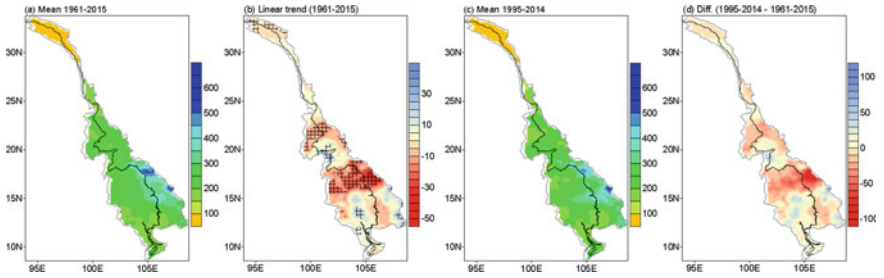

Fig. 2.5 Same as Fig. 2.1, but for Rx5day (mm) calculated based on daily precipitation from the APHRODITE

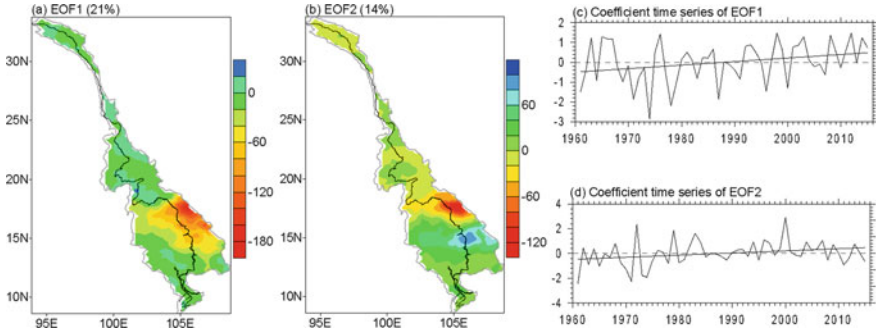

Fig. 2.6 Same as Fig. 2.2, but for Rx5day calculated based on daily precipitation from the APHRODITE

(2020) analyzed the temporal trend of drought over the LMRB during 1901–2019. They found that severe and exceptional droughts occurred more frequently during 1961–2019 compared to 1901–1960 with drought hotspots located in the middle and upper parts of the Lancang River Basin. About half of the lower reach of the LMRB has experienced an increase in severe and exceptional droughts, which are located principally in Thailand, east Cambodia, and part of Vietnam. The spatial distribution of mean and linear trend in the maximum length of dry spell: maximum number of consecutive days with RR < 1 mm (CDD) is shown in Fig. 2.7. There are two peak centres of CDD, one over the upper and the other over the center of the Mekong Basin. There is an increasing trend in CDD over the lower, middle and upper river basins. There is no significant trend in CDD during 1961–2015, but with clear inter-annual and inter-decadal variation in the CDD as shown by the EOF patterns (Fig. 2.8).

Changes in temperature extremes are shown by the maximum value of daily maximum temperature (TXx) and the minimum value of daily maximum temperature (TNn) (Figs. 2.9, 2.10, 2.11 and 2.12). Overall, there is an increase in both TXx and TNn, with the increases in TNn is robust than TXx. There is even a decrease in TXx over the southeast of the lower Mekong Basin.

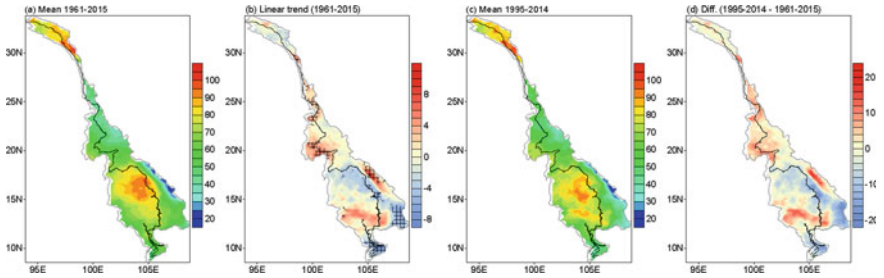

Fig. 2.7 Same as Fig. 2.1, but for CDD (days) calculated based on daily precipitation from the APHRODITE

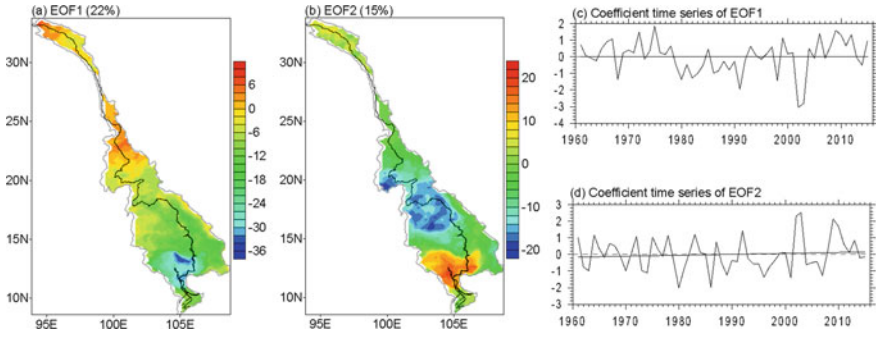

Fig. 2.8 Same as Fig. 2.2, but for CDD calculated based on daily precipitation from the APHRODITE

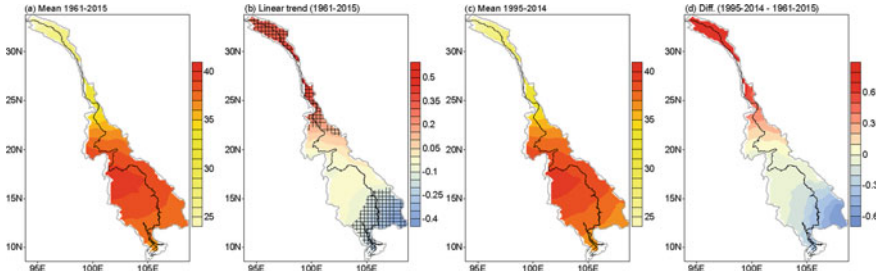

Fig. 2.9 Same as Fig. 2.1, but for TXx (°C) from gridded extremes indices, HadEX 3.0.3 (Dunn et al., 2020), which has been interpolated to the APHRODITE grid

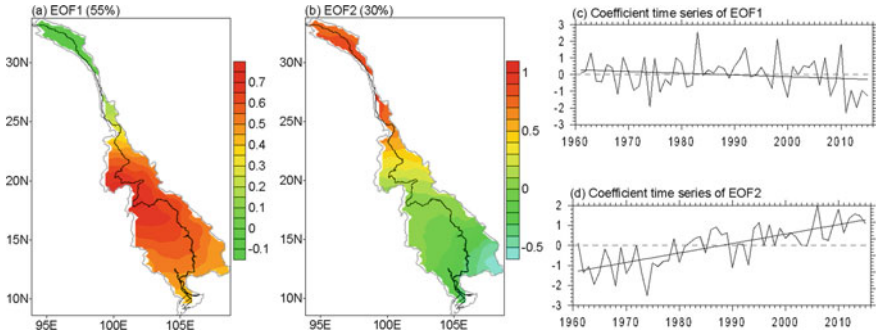

Fig. 2.10 Same as Fig. 2.2, but for TXx from HadEX 3.0.3 which has been interpolated to the APHRODITE grid

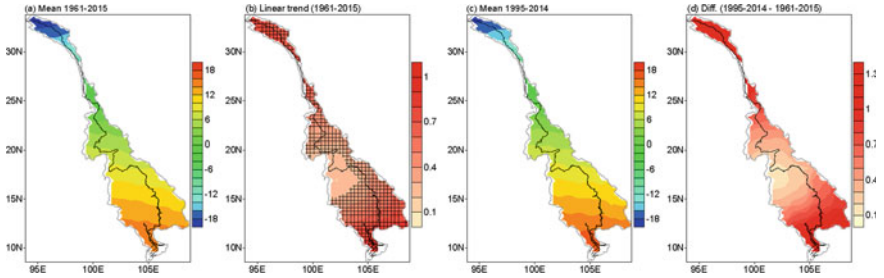

Fig. 2.11 Same as Fig. 2.9, but for TNn (°C) from HadEX 3.0.3 which has been interpolated to the APHRODITE grid

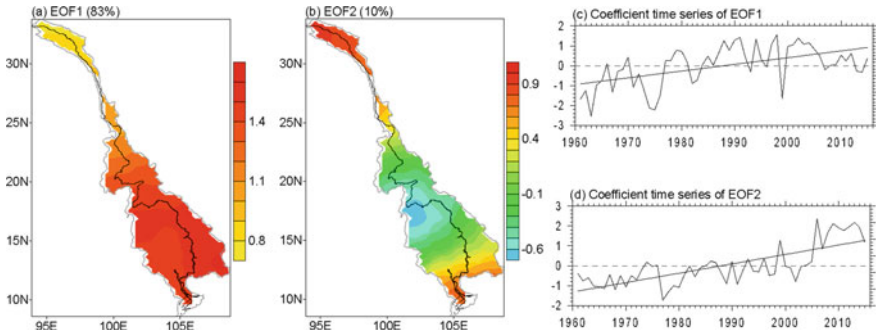

Fig. 2.12 Same as Fig. 2.11, but for TNn from HadEX 3.0.3 which has been interpolated to the APHRODITE grid

2.3 Projected Future Changes by the Ensemble of RCM Simulations

As shown in Sect. 2.2, the LMRB has experienced significant changes in climate in the last few decades. Understanding future climate change is crucial for the region to implement proper adaptation and mitigation measures. Application of high-resolution RCMs is particularly important over the Basin, which is characterized by unique weather/climate systems, complex coast lines and topography.

In this section, we report the projected climate change over the Basin based on an ensemble of twenty-first century projections with an RCM, the RegCM4 (Fu et al., 2021b). RegCM4 is developed and maintained by the Abdus Salam International Center for Theoretical Physics (Giorgi et al., 2012), and is one of the most widely used RCMs in the world.

RegCM4 was driven by five different CMIP5 GCMs and run over the CORDEX Phase II East Asia region, covering the whole of the Basin in the simulations. The GCMs are CSIRO-Mk3-6-0, EC-EARTH, HadGEM2-ES, MPI-ESM-MR, and NorESM1-M. The model is run at a grid-spacing of 25 km with the simulations covering 1971–2005, the historical period, using GHG concentrations, and 2006–2098, the future period under the RCP4.5 pathway (Gao et al., 2018). Here 1995–2014 is used as the reference period (present day), 2041–2060 and 2079–2098 as the mid- and end of the twenty-first century, respectively, following the periods used in the IPCC Sixth Assessment Report (IPCC AR6) (Lee et al., 2021).

The observation datasets of temperature and precipitation used to validate the present day simulations are the gridded observational dataset CN05.1 (Wu & Gao, 2013) over the Lancang River Basin, together with the APHRODITE (Yatagai et al., 2012) over the Mekong River Basin. The daily mean maximum and minimum temperatures employ also CN05.1 over the Lancang River Basin, but the Climate Prediction Center (CPC) Global Daily Temperature dataset (https://psl.noaa.gov/data/gridded/data.cpc.globaltemp.html) over the Mekong River Basin. The model outputs and the

CPC dataset are all bilinearly interpolated to the same grids of 0.25° (latitude) × 0.25° (longitude) as in CN05.1 and APHRODITE.

This section focuses on the ensemble mean of temperature and precipitation during the dry/cold season of November to March (NDJFM), the wet/warm season of May to September (MJJAS), and the whole year. Validation and inter-comparison of the models for both the present day period simulation and future changes between the driving GCMs and RegCM4 are provided. Two temperature extreme indices of TXx and TN, and two precipitation extreme indices of CDD and Rx5day are used to assess the simulation and projections in extremes by RegCM4.

2.3.1 Validation of the Present day Simulation

Surface air temperatures from the model simulations is compared against observations for the present day period of 1995–2014. Temperatures from the ensemble of the five GCM (ensG) and five RegCM4 (ensR) simulations along with observations in the dry and wet season, and the whole year, are shown in Fig. 2.13. In the observations (Fig. 2.13a–c), the lower reaches of the Basin is dominated by tropical climate, with prevailing temperatures warmer than 25.0 °C throughout the year. In the upper reaches in the north, both latitudinal and topographic dependences are found, with the lowest temperatures (<−10.0 °C) found during the dry season, and reaching >0 °C during the wet season. Regional mean temperatures in the dry and wet seasons, and the whole year are 19.9, 24.2, and 22.3 °C, respectively, over the Basin.

The broad pattern of the temperature from observation is reproduced in general by both ensG and ensR over the region of mainland Southeast Asia (MSEA), while ensR provides much finer spatial details, thus in better agreement with the observations (Fu et al., 2021b), although to a less extent in the River Basin (Fig. 2.13g–i). The temperature gradient due to the steep topography over MESA is realistically reproduced by ensR but not by ensG (Fu et al., 2021b). General cold biases prevail in both ensG and ensR during all seasons and the annual mean, greater in the dry than the wet season (not shown for brevity). Some small scattered warm biases are found along the eastern edge of the lower reach of the River Basin during the wet season and the whole year. Regional mean biases in the dry, wet seasons, and the whole year over the Basin are −2.9, −1.0, and −1.8 °C in ensG, and −2.7, −1.3, and −1.9 °C for ensR, respectively.

For precipitation, it is generally quite dry in the dry season over the Basin in observations, with less than 200 mm of precipitation over most places (Fig. 2.14a). With the monsoon dominating in the wet season, precipitation greater than 400 mm, with maxima reaching up to 1000 mm over the eastern part, is observed (Fig. 2.14b). The annual mean precipitation shows a similar pattern as the wet season but with larger values (Fig. 2.14c). The mean precipitation over the Basin in the dry season, the wet season, and the whole year are 118, 1018, and 1342 mm, respectively.

Similar to temperature, the general pattern, magnitude, and seasonal evolution of the observed precipitation are well reproduced over MSEA and LMRB by both

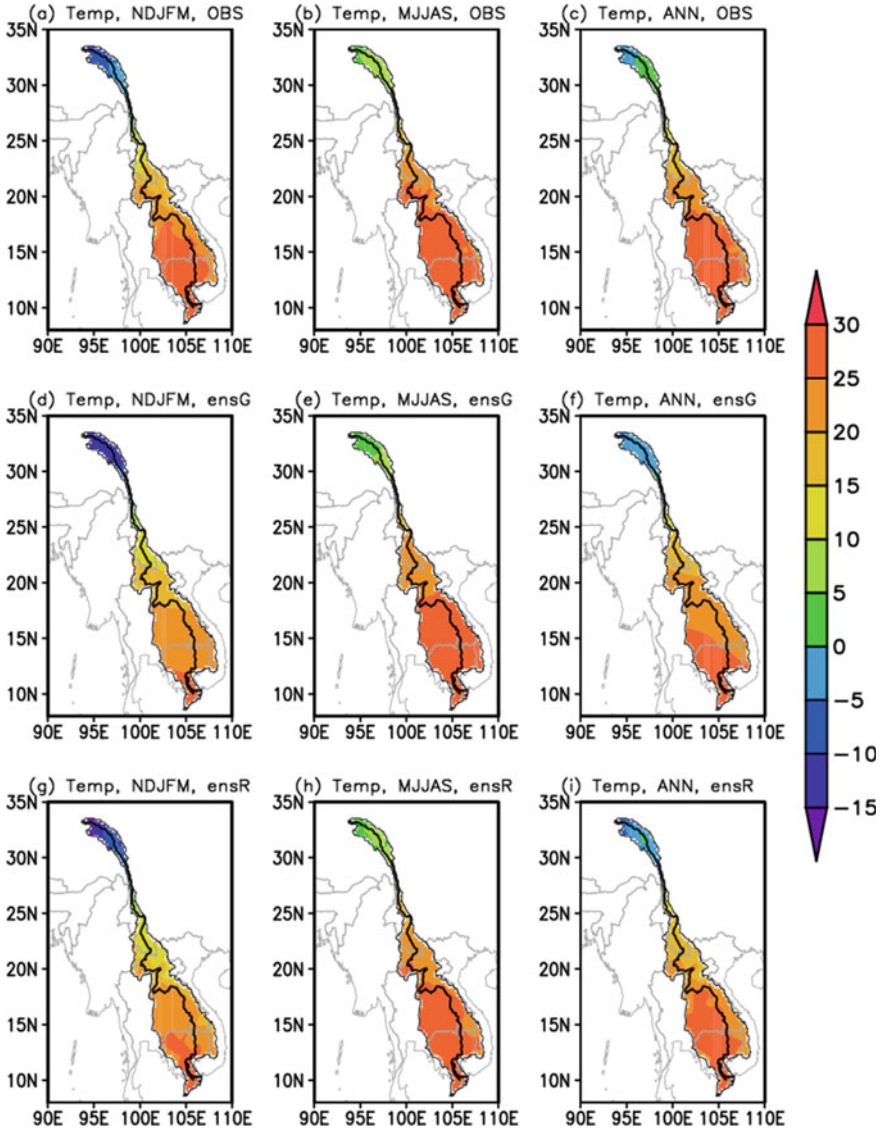

Fig. 2.13 Distribution of the present day (1995–2014) temperature over the LMRB. Observation in the dry season (**a**), the wet season (**b**), and the whole year (**c**); simulation by the ensemble of GCMs (ensG) in the dry season (**d**), the wet season (**e**), and the whole year (**f**); simulation by the ensemble of RegCM4 (ensR) in the dry season (**g**), the wet season (**h**), and the whole year (**i**). Unit: °C

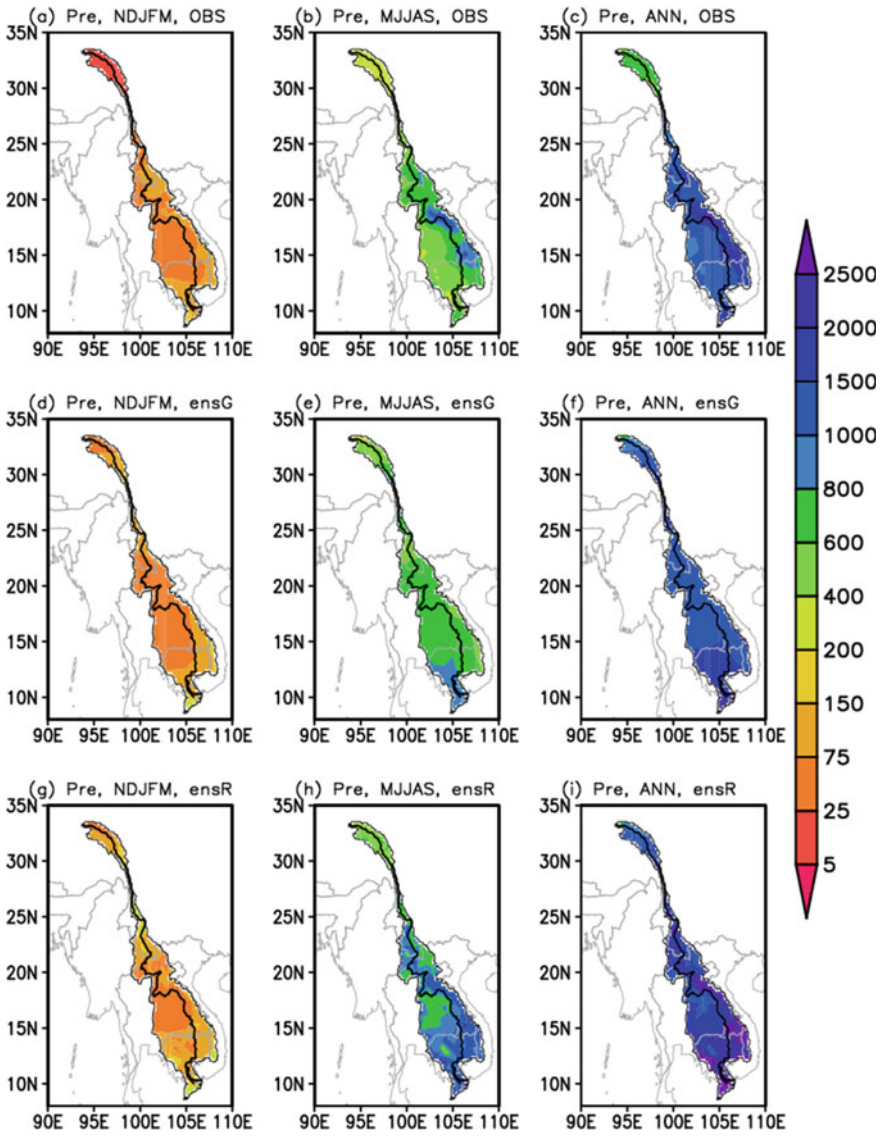

Fig. 2.14 Same as Fig. 2.13, but for precipitation. Unit: mm

ensG and ensR, while more regional details are provided by ensR compared to ensG (Fu et al., 2021b) (Fig. 2.14d–i). In addition, the ensR even exhibits finer spatial structure compared to the observation over the region, a result not surprising with the sparse distribution of observation sites there. A general overestimation is found for precipitation simulations in the model for both the dry and wet seasons, and the annual mean, more significant in ensR. Underestimation over places of the middle

Basin by both ensG and ensR in the dry season, and eastern part of the Basin by ensG in the wet season and the whole year, is found. Note that the "observational" precipitation may well underestimate the precipitation over the mountainous ranges due to the lack of observing sites in the high altitudes, and lack of the gauge undercatch corrections (Adam & Lettenmaier, 2003). Regional mean precipitation over the Basin in the dry and wet seasons, and the whole year, are 126, 1123, and 1432 mm for ensG, and 182, 1547, and 1982 mm for ensR, respectively.

The observated and the ensR simulated (ensG is not shown for brevity) extreme indices of TNn and TXx are presented in Fig. 2.15. For the TNn observation (Fig. 2.15a), the coldest temperatures are found over the head of the Basin (<−20 °C). Above zero temperatures are found in other places, and reach 15 °C in southern end of the Basin. The observed spatial pattern of TNn is well reproduced by ensR, although with general cold biases (Fig. 2.15b). The bias is the largest, >−9.0 °C, over the head regions, but this may be related to the sparse distribution of observing stations there. The bias is much smaller over the lower Basin (−3.0 °C). The regional mean values of TNn from the observation and ensR over the Basin are 7.6 and 3.3 °C, respectively.

The values of TXx (Fig. 2.15c, d) range from 20 to 30 °C over the upper and 30 to 35 °C over the lower Basin. Cold biases >5 °C exist over the head regions, and a mix of cold and warm biases within ±2 °C is found over other places. Regional mean values of TXx over the Basin for the observations and ensR are 35.5 and 34.5 °C, respectively.

The observed CDD shows the smallest values (30–40 d) along the eastern edge of the Basin (Fig. 2.16a). Values >50 d are located over the head regions, most of Cambodia, and eastern Thailand. The general CDD spatial pattern is reproduced well in ensR, but with prevailing underestimations (Fig. 2.16b), likely due to the too many days of drizzle as commonly found in climate models. The regional mean from observation is 46 d, while in ensR it is 30 d over the Basin.

The spatial distributions of Rx5day shows strong topographic dependences, with greater values >150 mm mostly along the mountain ranges over the border areas of Vietnam and Laos (Fig. 2.16c). The topographic effect is more pronounced in ensR, characterised by greater values, and more extended areas along the Truong Son Mountain (Fig. 2.16d). A general overestimation of Rx5day is simulated (figure not shown for brevity), consistently with the mean precipitation. The average over the Basin for ensR is 177 mm, greater than the 114 mm in the observations.

2.3.2 Future Changes

Figure 2.17 shows the projected temperature change over the Basin in the dry and wet seasons, and the whole year by the end of the twenty-first century. Substantial warming is found, more significant in the dry compared to the wet season and over the upper compared to the lower Basin. In the dry season, the warming in ensG is evenly distributed, with values >2.2 °C over most of the Basin (Fig. 2.17a), while in ensR,

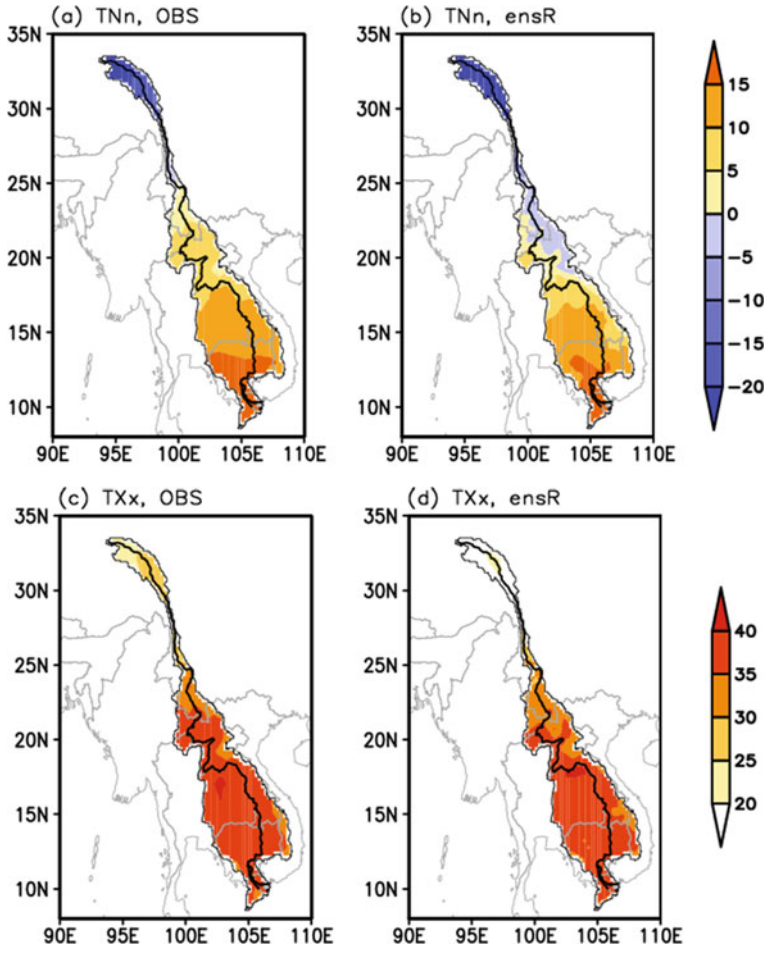

Fig. 2.15 Distribution of present day (1995–2014) TNn over the LMRB in observation (**a**) and simulated by ensR (**b**); **c**, **d** same as **a**, **b**, but for TXx. Unit: °C

large sub-regional variability is found, with >3.0 °C values over the source regions with high altitudes, and <2.0 °C values over the lower Basin (Fig. 2.17d). This effect of warming amplification with elevation has been found in previous studies, mostly due to the response to the reduction of snow cover (e.g. Giorgi et al., 1997; Fu et al., 2021a). The values of regional mean warming over the Basin for ensG and ensR are 2.3 °C (with inter-model spread of 1.4–3.6 °C) and 1.9 °C (0.7–2.7 °C), respectively (Table 2.2). Thus lower region-mean warming and inter-model spread are found in RegCM4, likely due to the same physics schemes used in all runs, which modulate the effect of lateral boundary forcings.

The warming is lower in the wet season (Fig. 2.17b, e) for both ensG and ensR. Again, lower warming is simulated in ensR in general compared to ensG. In ensG,

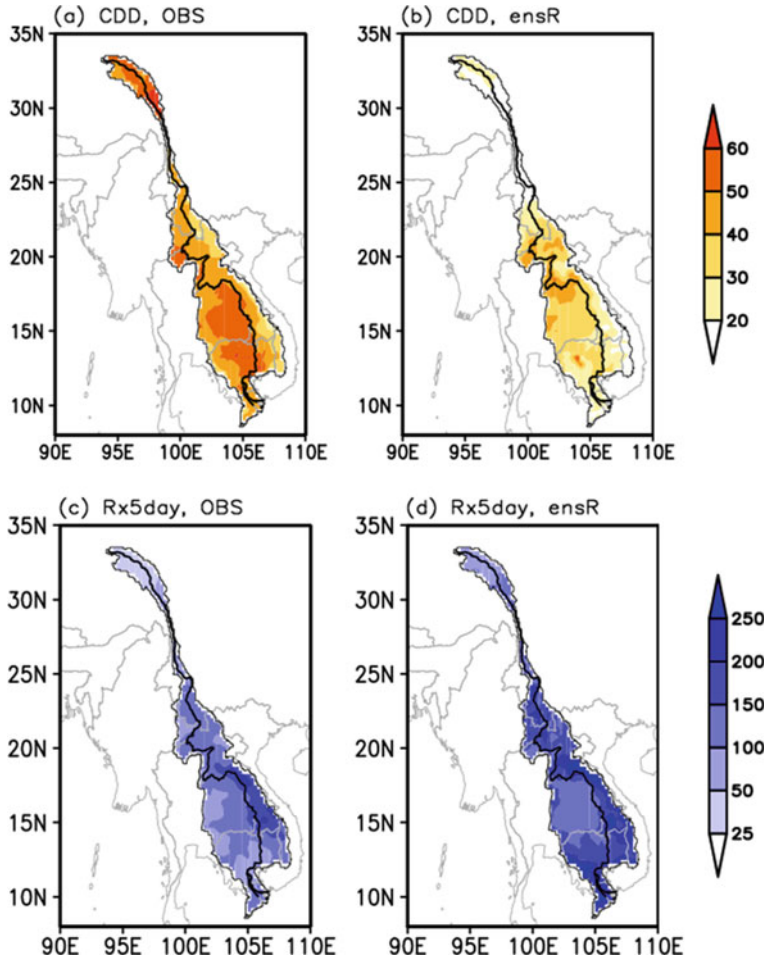

Fig. 2.16 Same as Fig. 2.15, but for CDD and Rx5day. Units are d for **a**, **b** and mm for **c**, **d**

the least warming values <1.6 °C is found over the lower Basin (Fig. 2.17b). The warming is greater over the mid- and upper-Basin, with values ranges from 2.0 to 2.4 °C. For ensR, lower than 1.6 °C warming are simulated over most of the Basin, except in the head regions (Fig. 2.17e). The regional mean warming over the Basin is 1.9 °C (1.4–2.5 °C) and 1.4 °C (1.0–2.2 °C) for ensG and ensR, respectively.

The projected annual mean temperature changes, either the magnitude or distribution, lie between the dry and wet seasons (Fig. 2.17c, f). In ensG, the warming ranges mostly from 2.1 to 2.4 °C over the whole Basin (Fig. 2.17c). In ensR, more pronounced warming in the north, with the largest values >2.4 °C, and lower in the south, in the range of 1.4–1.6 °C, are found (Fig. 2.17f). The projected mean

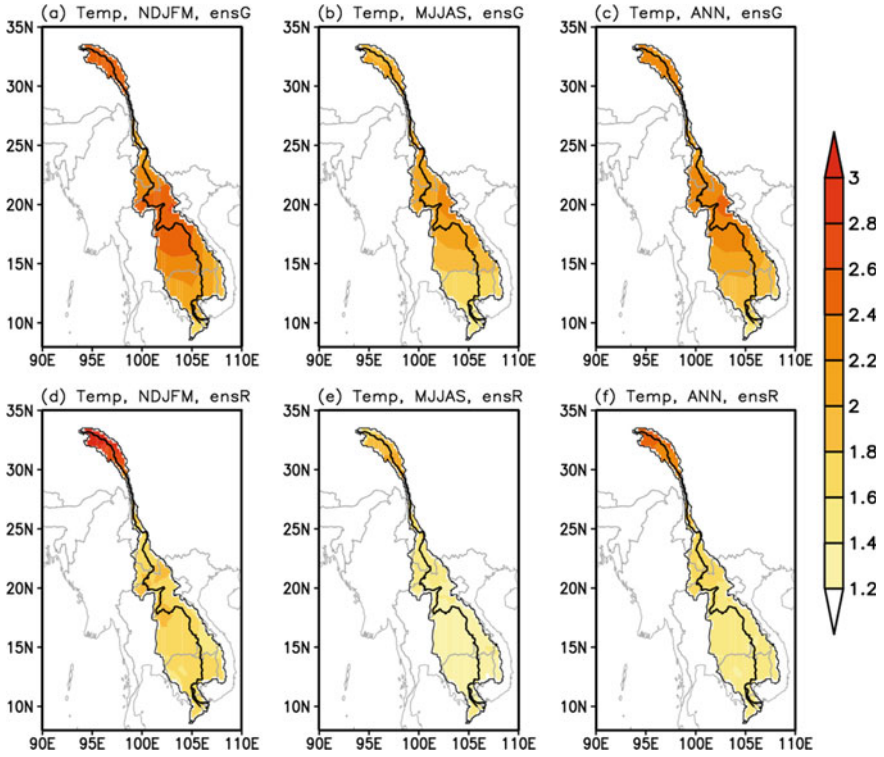

Fig. 2.17 The projected changes of temperature by the end of the twenty-first century (2079–2098) under RCP4.5 over the LMRB. By ensG in the dry (**a**) and wet (**b**) seasons, and the whole year (**c**); by ensR in the dry (**d**) and wet (**e**) seasons, and the whole year (**f**). The sign of the changes for the inter-models and cross simulations are in good agreements, thus not shown for brevity. Unit: °C

Table 2.2 Regional mean changes temperature and precipitation for the dry (NDJFM), wet (MJJAS) seasons, and the annual mean over LMRB projected by ensR and ensG under RCP4.5 in the mid- (2041–2060) and end (2079–2098) of the twenty-first century (relative to the present day of 1995–2014)

Variable		NDJFM (ensG/ensR)	MJJAS (ensG/ensR)	ANN (ensG/ensR)
Temperature (°C)	2041–2060	1.5/1.3 (0.9–2.3/0.7–1.7)	1.3/0.9 (1.1–1.6/0.5–1.5)	1.4/1.1 (1.1–1.9/0.9–1.6)
	2079–2098	2.3/1.9 (1.4–3.6/0.7–2.7)	1.9/1.4 (1.4–2.5/1.0–2.2)	2.1/1.6 (1.5–3.0/1.0–2.4)
Precipitation (%)	2041–2060	5/4 (−10–30/−3–12)	2/−2 (−2–7/−4–1)	3/1 (−2–7/−2–3)
	2079–2098	9/7 (−16–33/−3–15)	4/−2 (−4–9/−5–0)	6/1 (2–13/−2–4)

Note Values in the brackets are the minimum–maximum in the five GCMs/RegCM4 simulations

changes of annual temperature for ensG and ensR are 2.1 °C (1.5–3.0 °C) and 1.6 °C (1.0–2.4 °C), respectively, over the Basin.

The regional averaged warming and the inter-model/cross simulation spreads of ensG and ensR during the mid- twenty-first century over the Basin are also presented in Table 2.2. The changes are in general consistent with the end of the century but to smaller values, and with greater warming during the dry season, and in ensG compared to ensR.

Figure 2.18 presents the precipitation changes at the end of the twenty-first century. For ensG during the dry season, a prevailing increase over the basin is found except in the southeastern corner (Fig. 2.18a). Values of the increase are mostly >15%, with maxima reaching over 20%. The inter-model agreement of the sign of change is high in the mid- and upper Basin, with greater increases there. The change of ensR shows consistencies, except for the finer spatial detail (Fig. 2.18d). Regional changes of precipitation for ensG and ensR are 9% (−16 to +33%) and 7% (−3 to +15%), respectively, over the Basin (Table 2.2).

During the wet season, general increases of precipitation in ensG, with the largest increase by >10% over the Mekong Delta are found (Fig. 2.18b), excerpt the slight

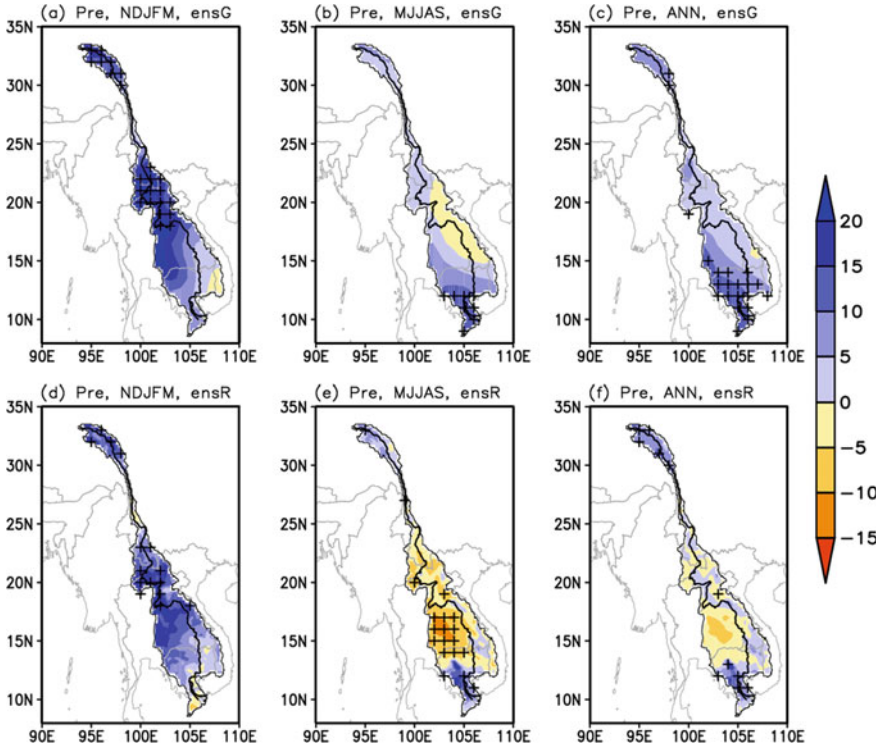

Fig. 2.18 Same as Fig. 2.17, but for precipitation. The cross indicates at least four out of the five GCMs/RegC4 simulations agree on the sign of change. Unit: %

decreases by <5% in eastern part of the Basin. The changes show low inter-model agreements in most places, except over the Mekong Delta with larger increases. Meanwhile, the projected precipitation exhibits a general decrease in ensR over almost all the places, with good agreement in the change sign over the places with larger changes (>−5%) (Fig. 2.18e). The largest decrease by 10–15% is mainly located in southeastern Thailand. The regional mean change is positive, by 4% (−4 to +9%) over the Basin in ensG, but negative by −2% (−5 to 0%) in ensR (Table 2.2). It is difficult to ascertain the cause of the difference, but previous studies have shown, that models with higher resolution tend to represent the dynamics of the East Asia monsoon better (Gao et al., 2006, 2012), and this may have an effect on the changes projected.

In general, the pattern of annual mean precipitation change is consistent with those in the wet season. For ensG, a general increase is found over the Basin, with the largest increase greater than >5%, and good inter-model agreements over the southwestern edge of the Basin (Fig. 2.18c). For ensR, a mix of positive/negative changes within ~ ±5% are found, with low coress-simulation agreements over almost all of the region (Fig. 2.18f). The regional mean changes in annual mean precipitation for ensG and ensR are 6% (+2 to +13%) and 1% (−2 to +4%), respectively, over the Basin (Table 2.2).

The projected regional mean precipitation changes over the Basin during the mid-twenty-first century are about half as large as by the end of the century for ensG, and during the dry season for ensR. Closer values for the changes in ensR between the mid- and end of the century during the wet season and the whole year (Table 2.2).

Figure 2.19a, b show the distributions of projections in the temperature extreme indices, TNn and TXx, at the end of the twenty-first century from ensR. The change of both TNn and TXx show significant increases under the warming, indicating fewer cold events and more frequent heat waves in the future. For TNn, the increases are greater over the high-latitude and high-altitude regions, with values of increase >3.0 °C (Fig. 2.19a). This is possibly caused by the reduction in snow cover and thus the snow albedo feedback effect. The increase tend to be much lower to the south, range from ~1.0 to 2.0 °C. The increases in TXx show inhomogeneously distributions (Fig. 2.19b), with values greater than 2.0 °C found over the upper and middle Basin, and less than 1.4 °C over the Mekong Delta in the south. Regional mean changes for TXx and TNn are 1.8 °C (0.9–2.6 °C) and 2.1 °C (1.7–2.9 °C), respectively, over the Basin (Table 2.3).

Changes in CDD and Rx5day by the end of the twenty-first century are shown in Fig. 2.19c, d, respectively. For CDD, a pronounced increase over a broad area in the middle and lower Basin, including northern Laos, eastern Thailand, and most of Cambodia, is found, with increases ranges from 2 to 4 days (10–25%) in correspondence with the generally decreased precipitation in the wet season and consequently the whole year (Fig. 2.18), although with low cross simulation agreements. Meanwhile, CDD is projected to decrease by 2–4 days over the upper Basin and the eastern part of middle Basin.

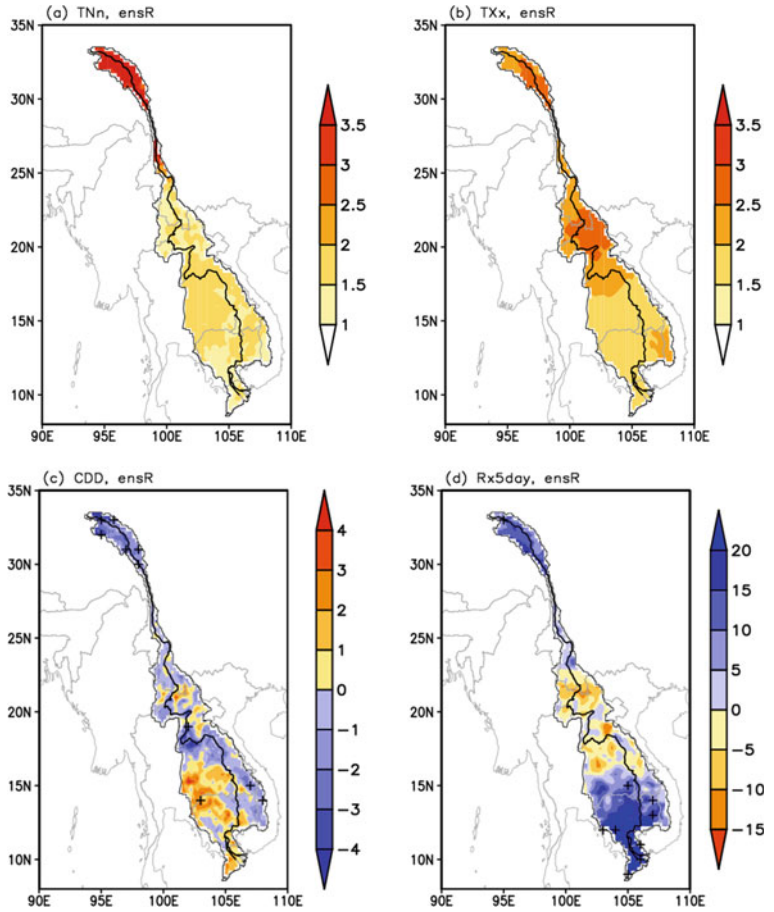

Fig. 2.19 The projected changes of TNn (**a**), TXx (**b**), CDD (**c**) and RX5day (**d**) by the end of the twenty-first century under RCP4.5 over the MRB in ensR. The cross indicates at least four out of five GCMs/RegCM4 simulations agree on the sign of change. Units are: °C, °C, day, and %, respectively

Table 2.3 Projected regional mean changes of TNn, TXx, CDD, and Rx5day over LMRB by ensR at the mid- (2041–2060) and end (2079–2098) of the twenty-first century under RCP4.5

Periods/variable	TNn (°C)	TXx (°C)	CDD (days)	Rx5day (%)
2041–2060	1.3 (1.1–1.8)	1.5 (1.1–2.0)	0.4 (−0.8–1.8)	5.6 (0.2–14.5)
2079–2098	1.8 (0.9–2.6)	2.1 (1.7–2.9)	−0.3 (−1.8–1.4)	8.4 (−1.1–16.8)

Note The values in brackets are the minimum–maximum in the five GCMs/RegCM4 simulations

The Rx5day is projected to increase by 10–25% over the upper and lower Basin, with the largest increase >50% found over the Mekong Delta with good cross simulation agreements (Fig. 2.19d). For the middle Basin, the change is a decrease by 5–15%. Comparison with change of CDD (Fig. 2.19c), both increases in CDD and Rx5day are found over lower Basin, suggesting the greater risk of the increase in both flood and drought disasters over the area in the future. Regional mean changes of CDD and Rx5day are −0.3 d (−1.8 to +1.4 d) and 8.4% (−1.1 to +16.8%), respectively, over the LMRB (Table 2.3).

2.4 Multi-model Simulations, Projections and Uncertainty Analysis

2.4.1 Evaluations of Historical Simulations

The spatial distributions of annual total precipitation and annual mean temperatures from the 16 CMIP6 models (Table 2.4) and APHRODITE observations over the LMRB are shown in Figs. 2.20 and 2.21. Generally, both the observed annual total precipitation and annual mean temperature exhibit an increasing gradient from the north to south of the Basin. Most CMIP6 models can reproduce the spatial distribution of annual temperature over the LMRB, despite there being slightly consistent cold biases for most models. The multi-model mean results are notably similar to observations in most regions, and the biases are relatively smaller than those of most individual models. In contrast, precipitations estimated by various CMIP6 models exhibit larger differences, and most models overestimate the precipitation compared with the APHRODITE observations. The BCC-CSM2-MR, CESM-WACCM, CESM2, CanESM5, GFDL-ESM4, UKESM1-0-LL models especially overestimate the annual total precipitation in the southern part of the LMRB. Similarly, CMIP6 model mean precipitation estimation behaves better than most individual models.

The agreement between model-simulated and observed precipitation and temperature was further evaluated through the Taylor diagrams, considering their spatial correlations, root-mean-square differences, and the amplitude of their variations (represented by their standard deviation). Figure 2.22 shows the precipitation and temperature Taylor diagram for the climatology of the period 1995–2014 for individual CMIP6 models and model mean over the LMRB. Based on the Taylor diagrams, most models show good performance for temperature, with a correlation coefficient typically >0.9 and a close match to the APHRODITE observations. Also, most of the models exhibit a ratio of the standard deviations that is close to 1, and the centred pattern RMSE difference range was 0.2–0.3. Comparatively, CAMS-CSM1-0, CESM2-WACCM, CESM2, and UKESM1-0-LL perform better over the LMRB. IPSL-CM6A-LR and FGOALS-g3 present relatively poor performance compared to

Table 2.4 List of 16 CMIP6 models in this study and their spatial resolution

Model name	Modeling center	Spatial resolution
BCC-CSM2-MR	Beijing Climate Center, China	320 × 160
CAMS-CSM1-0	Chinese Academy of Meteorological Sciences, China	320 × 160
CESM2-WACCM	National Center for Atmospheric Research, Climate and Global Dynamics Laboratory, United States	288 × 192
e	National Center for Atmospheric Research, Climate and Global Dynamics Laboratory, United States	288 × 192
CNRM-CM6-1	National Centre for Meteorological Research, France	256 × 128
CNRM-ESM2-1	National Centre for Meteorological Research, France	256 × 128
CanESM5	Canadian Centre for Climate Modelling and Analysis, Environment and Climate Change Canada, Canada	128 × 64
EC-Earth3-Veg	EC-Earth Consortium, Europe	512 × 256
EC-Earth3	EC-Earth Consortium, Europe	512 × 256
FGOALS-g3	LASG, Institute of Atmospheric Physics, Chinese Academy of Sciences, China	180 × 80
GFDL-ESM4	National Oceanic and Atmospheric Administration, Geophysical Fluid Dynamics Laboratory, United States	288 × 180
IPSL-CM6A-LR	Institut Pierre Simon Laplace, France	144 × 143
MIROC-ES2L	JAMSTEC (Japan Agency for Marine-Earth Science and Technology), AORI (Atmosphere and Ocean Research Institute, The University of Tokyo), NIES (National Institute for Environmental Studies) and R-CCS (RIKEN Center for Computational Science), Japan	128 × 64
MIROC6	JAMSTEC, AORI, NIES and R-CCS, Japan	256 × 128
MRI-ESM2-0	Meteorological Research Institute, Japan	320 × 160
UKESM1-0-LL	Met Office Hadley Centre, United Kingdom	192 × 144

other models. In contrast, most CMIP6 models do not perform very well in representing historical precipitation. The correlation coefficient is between 0.2 and 0.7, RMSE is between 0.9 and 1.5 and the standard deviation is around 1. The correlation coefficients of only three models including EC-Earth3, EC-Earth3-Veg, and IPSL-CM6A-LR are greater than 0.6. These three models along with CMIP6 mean were taken out for future investigation as shown in Fig. 2.23. It shows that the annual total precipitation of the APHRODITE is around 1200 mm whereas the annual total precipitation of three CMIP6 models and model mean are around 1450–1550 mm. This indicates that even the best CMIP6 models overestimate precipitation by more than 25% and most CMIP6 models do not perform well in precipitation estimation in the southeast Asian region. Therefore, in this study, precipitation projections are not further evaluated for the future scenarios for the LMRB. Dynamic downscaling or bias correction techniques can be applied to derive better precipitation simulations in the future but they are beyond the scope of this study.

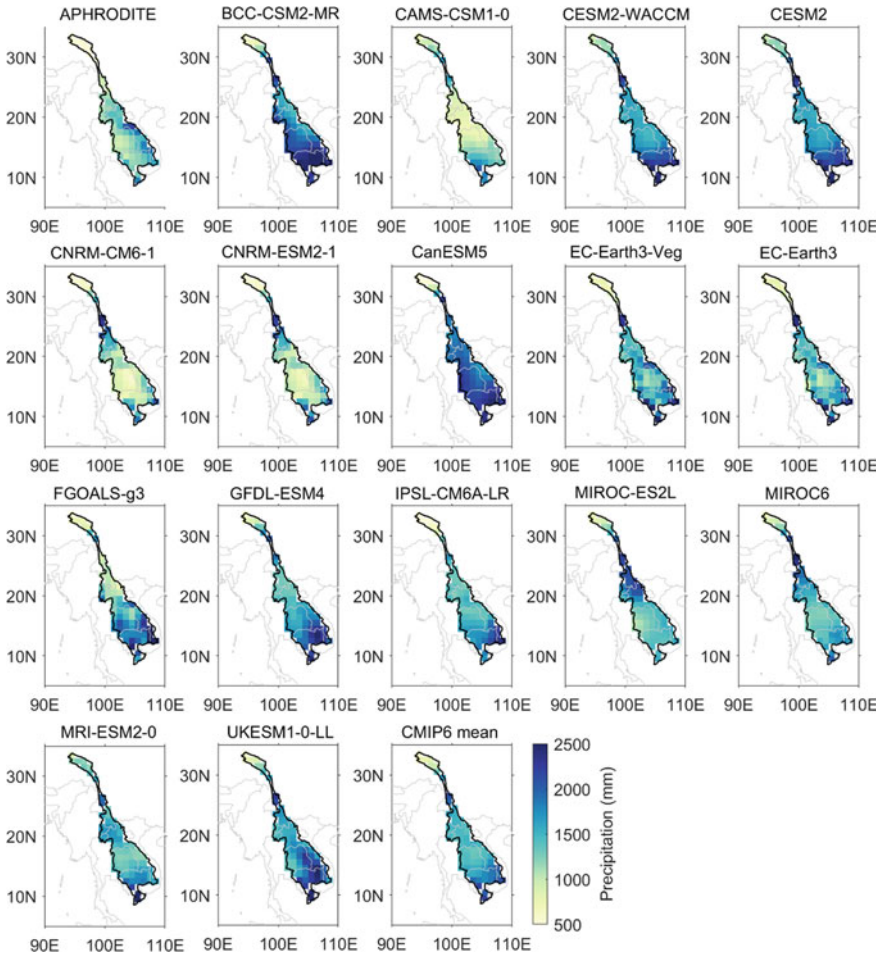

Fig. 2.20 Spatial distributions of annual total precipitation from 16 CMIP6 models, ensemble averages, and APHRODITE observations over the LMRB for the 1995–2014 average

Figure 2.24 shows 10-year moving average values for annual mean temperature for the ensemble of the 16 models and for the observations. The analysis shows that the observed annual mean temperature lies within the 5th–95th percentile range of CMIP6 multi-model ensembles, implying that there is consistency between the observed record and the CMIP6 models. Additionally, the CMIP6 historical simulations can reproduce the observed annual temperature warming trends in the LMRB, although with a slight positive bias.

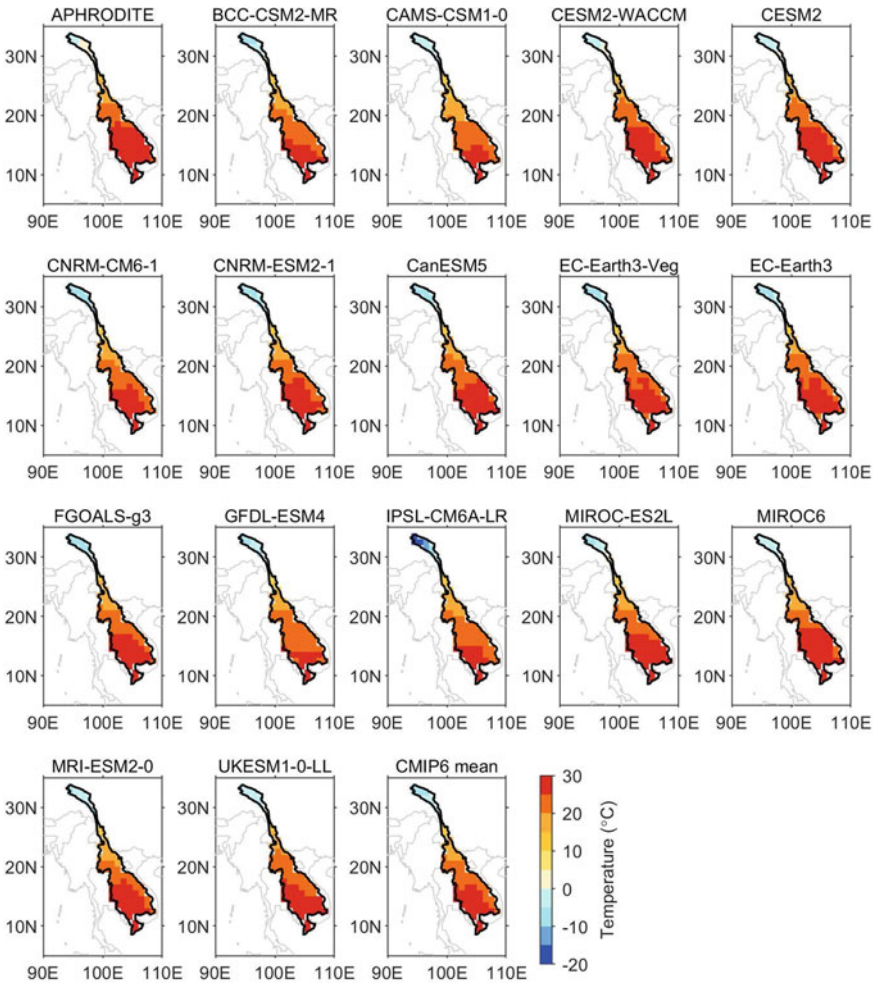

Fig. 2.21 Spatial distributions of annual mean temperatures from 16 CMIP6 models, ensemble averages, and APHRODITE observations over the LMRB for the 1995–2014 average

2.4.2 Projected Changes in Temperature for the Twenty-First Century

2.4.2.1 Annual Mean Temperatures

In this section, future changes in temperature over LMRB in the twenty-first century under the SSP1-2.6, SSP2-4.5, SSP3-7.0, and SSP5-8.5 pathways were presented. Figure 2.25 depicts the spatial patterns of climatological changes in mean temperature, utilizing multi-model ensemble averages for two distinct periods, mid-century

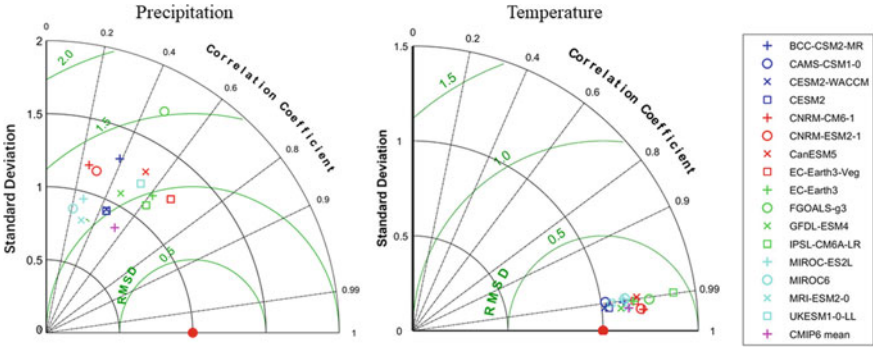

Fig. 2.22 Taylor diagrams for climatological of annual precipitation and temperature over the LMRB comparing each of the CMIP6 models and the observations for the period 1995–2014. The radial coordinate is the magnitude of the standard deviation (denoted by black arcs). The concentric green semi-circles denote root-mean-square difference (RMSD) values. The angular coordinate shows the correlation coefficient (denoted by dotted black lines)

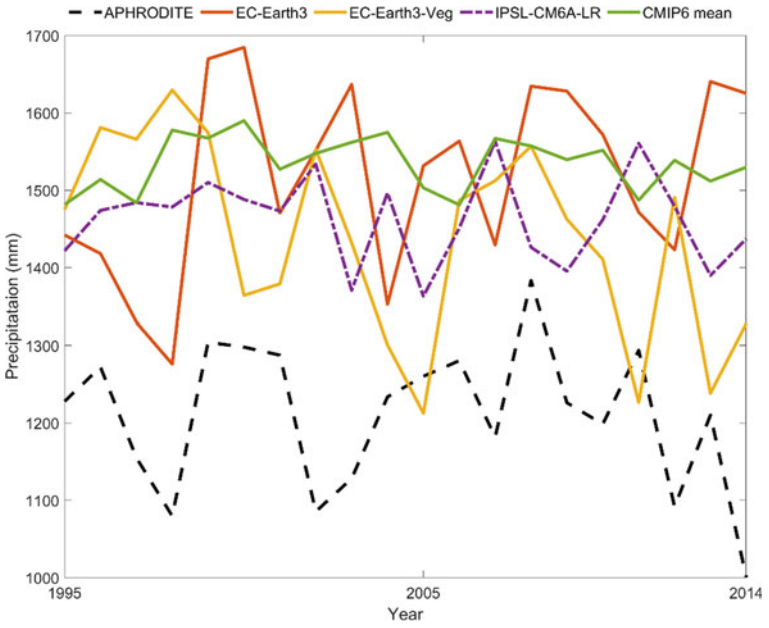

Fig. 2.23 Annual total precipitation for the three best models (correlation coefficient >0.6), CMIP6 model mean and APHRODITE for 1995–2014

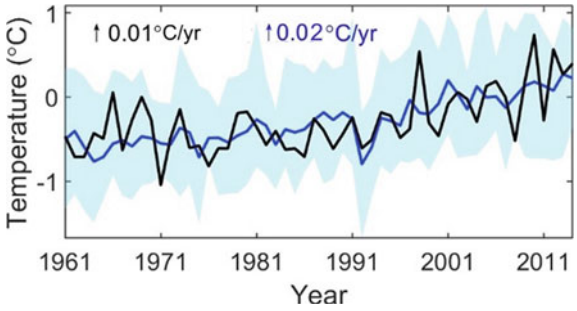

Fig. 2.24 Time series of 10-year moving average annual surface mean temperature from the CMIP6 models and APHRODITE observational dataset during 1961–2014 (blue line and shading: CMIP6; black line: APHRODITE). The trends are calculated for the observations and the CMIP6 ensemble mean during 1961–2014. The shading indicates the ensemble spread (range between the 5th and 95th quantiles). The liner trends are given on top of the time series

(2041–2060) and end of the century (2081–2100), relative to the baseline (1995–2014). The multi-model ensemble mean has been developed for assessing the projected changes.

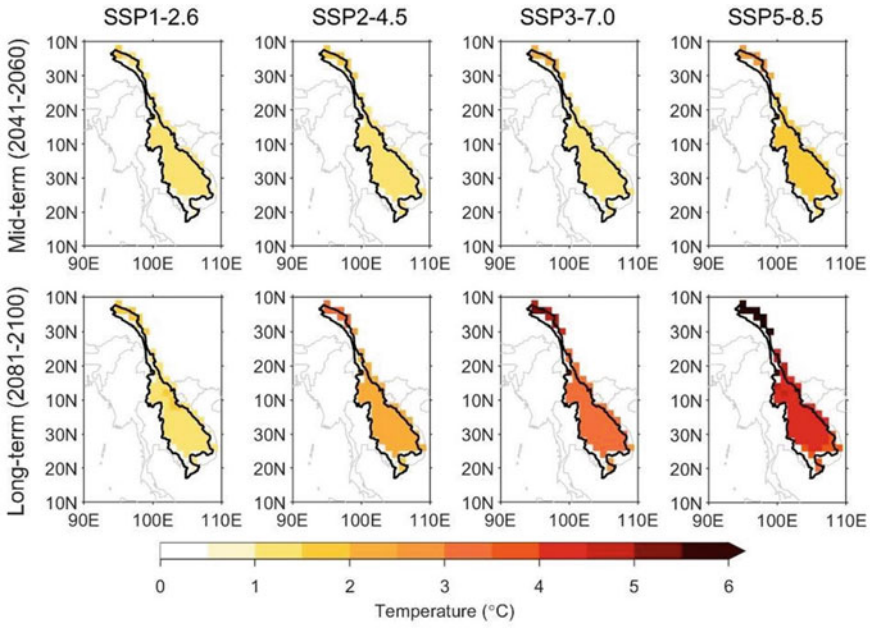

Fig. 2.25 Spatial distribution of changes in annual mean temperature over the LMRB in mid-(2041–2060) and long-term (2081–2100) periods of the twenty-first century, relative to 1995–2014, under the SSP1-2.6, SSP2-4.5, SSP3-7.0, and SSP5-8.5 scenarios. Unit: °C

Projections from the CMIP6 ensemble mean indicate a persistent trend of temperature elevation across the LMRB. In the simulations, the Lancang River Basin will undergo the greatest absolute temperature increases, while the Southern Mekong River Basin will experience weaker warming. Throughout the mid-term period (2041–2060), different scenarios do not lead to dramatically changed temperature responses under SSP1-2.6, SSP2-4.5, and SSP3-7.0, with most regions observing a temperature elevation lesser than 1.5 °C. However, under the SSP5-8.5 scenario, the temperature increase is generally about 2.0 °C over the Basin, and the increase exceeds 2.0 °C in the Lancang River. By the end of the this century (2081–2100), the projected annual mean temperature increase is significantly larger than the increase for the mid-term period (2041–2060) in all four scenarios. Meanwhile, the increasing temperatures under the SSP5-8.5 and SSP3-7.0 scenarios are more pronounced than under SSP2-4.5 and SSP1-2.6. The temperature changes under the low-forcing sustainability pathway (SSP1-2.6 scenario) are relatively small, with increases generally remaining within 2.0 °C. Compared with SSP1-2.6, ubiquitous temperature increases of 0.7–1.7 and 1.7–3.5 °C are apparent under the SSP2-4.5 and SSP3-7.0 projections, respectively. Additionally, under the SSP5-8.5 scenario, the increase exceeds 4.0 °C over most of the LMRB, and it exceeds 6.0 °C over the Lancang River Basin.

Temporal evolution from 1901 to 2100 of the annual mean temperature changes derived from the multi-model mean over the LMRB is shown in Fig. 2.26, together with their inter-model spreads. All the scenarios exhibit significantly increasing temperatures during the twenty-first century. The SSP5-8.5 scenario exhibits the largest increasing trend, at a rate of 0.06 °C/yr. The SSP3-7.0 and SSP2-4.5 scenarios each show a smaller increasing trend, at a rate of 0.04 and 0.03 °C/yr, respectively. As the lowest-pathways scenario, the SSP1-2.6 experiment projects the lowest rate (0.02 °C/yr) of temperature increase.

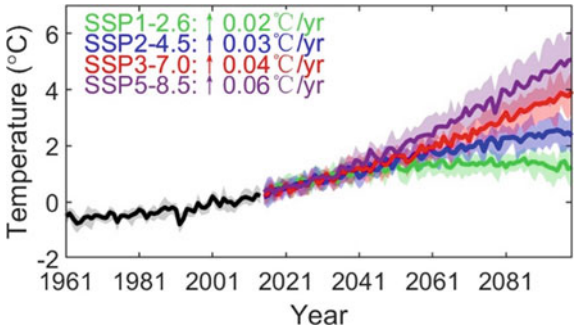

Fig. 2.26 Time series of changes in annual mean temperature over the LMRB during 1961–2100 relative to the period 1995–2014. The black, green, blue, red, and purple curves represent the results of the CMIP6 ensemble mean for the historical period and for the SSP1-2.6, SSP2-4.5, SSP3-7.0, and SSP5-8.5 scenarios, respectively. The shaded areas are the spreads from the 25th to the 75th percentiles of the annual mean temperatures

2.4.2.2 Projected Changes in Seasonal Temperatures

To further quantify the seasonal temperature changes with respect to the historical period for mid- and long-term periods of the twenty-first century under SSP1-2.6, SSP2-4.5, SSP3-7.0, and SSP5-8.5 scenarios, the seasonal temperature changes were summarized and compared by boxplots (Fig. 2.27), where the inter-model range is represented by the vertical whiskers in the box. In general, the seasonal temperature changes show a large and continuous increase with the increase of future emissions, and the uncertainty ranges also gradually increase. For both mid-term and long-term periods, spring (March–May, around 5.6 °C under SSP5-8.5) and summer (June–August, around 5.1 °C under SSP5-8.5) show greater temperature changes than winter (December–January, around 4.5 °C under SSP5-8.5) and fall (September–November, around 3.9 °C under SSP5-8.5) relative to historical periods. Under the scenarios of SSP2-4.5, SSP3-7.0, and SSP5-8.5, the temperature changes of the four seasons in the long-term period will increase significantly compared with that in the mid-term period. For SSP1-2.6, the CMIP6 models exhibit few temperature increases between the long-term period and the mid-term period. And in winter and summer, CMIP6 models show a smaller model range of temperature increases in the long-term period than mid-term period, which indicates a smaller uncertainty in long-term projections under SSP1-2.6.

Figure 2.28a, b show the pattern of the CMIP6 mean inter-seasonal temperature changes for the mid- and long-term period, respectively. For RCP4.5, the CMIP6 mean displays the possibility of large temperature increases during December, January, April, and May under four future scenarios, and smaller increases during July and August. The CMIP6 mean projects quite a large increase in temperature during the long-term period under SSP2-4.5, SSP3-7.0, and SSP5-8.5. It can be seen from Fig. 2.28b that the largest increase in temperature (greater than 4.5 °C under SSP5-8.5) is projected for April and May, while temperatures increase by smaller amounts (around 4.0 °C under SSP5-8.5) in July and August. In the SSP1-2.6 case, the CMIP6 mean shows the possibility of a lower increase in temperature than those under the medium and high future scenarios.

2.4.2.3 Projected Changes in Temperature Extremes

Four temperature extremes indices (Table 2.5), as recommended by the Expert Team on Climate Change Detection and Indices (ETCCDI), have been chosen to evaluate future changes in daily maximum (TX) and daily minimum (TN) temperatures from 1951 to 2099. These encompass three hot indices (annual maximum value of TX, TXx; the percentage of warm days, TX90p; and the percentage of warm nights, TN90p) and one cold index (annual minimum value of TN, TNn), which together can characterize the intensity and frequency of temperatures extremes.

Figures 2.29 and 2.30 depict the spatial distributions of projected changes in indices of temperature extremes over the LMRB during the mid- and long-term periods of the twenty-first century. Each index of extreme temperatures is are

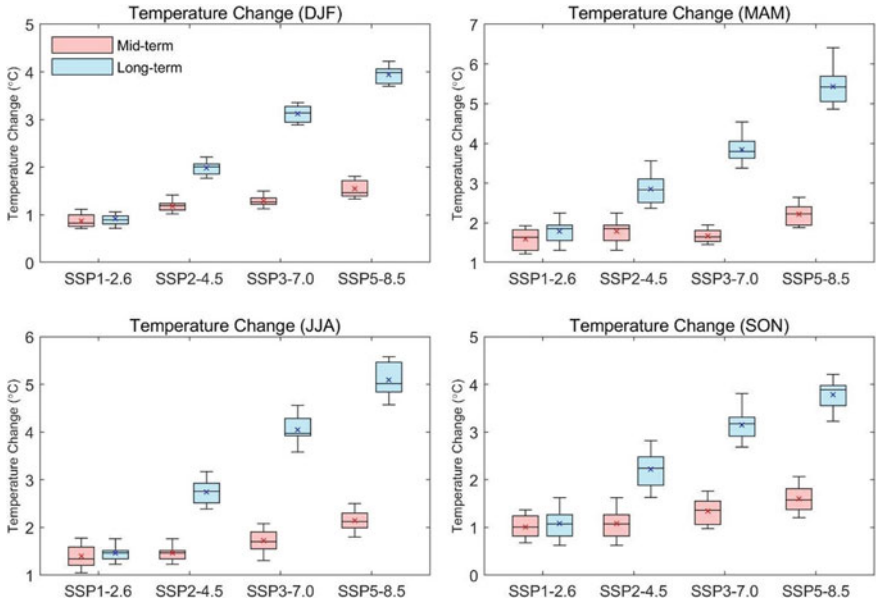

Fig. 2.27 The box and whisker plots show seasonal temperature changes for mid-term (2041–2060) and long-term (2081–2100) periods of the twenty-first century with respect to the base period 1995–2014 under SSP1-2.6, SSP2-4.5, SSP3-7.0, and SSP5-8.5 scenarios. Boxes indicate the interquartile model spread (25th and 75th quantiles), with the horizontal line indicating the ensemble median and the whiskers showing the total inter-model range. The ensemble means are indicated using red and blue crosses

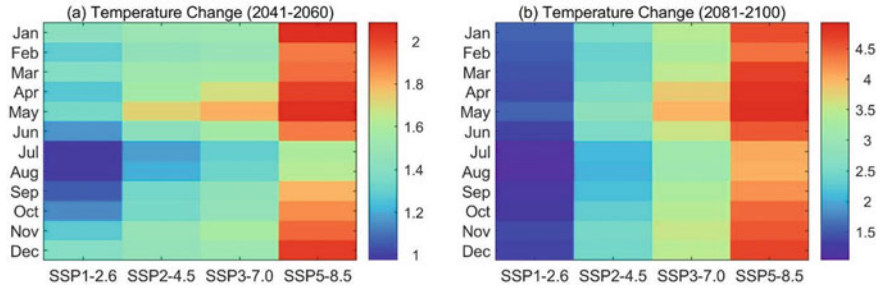

Fig. 2.28 Inter-seasonal temperature changes illustrated by the multi-model ensemble for **a** mid-term (2041–2060) and **b** long-term (2081–2100) periods of the twenty-first century, relative to 1995–2014, under the SSP1-2.6, SSP2-4.5, SSP3-7.0, and SSP5-8.5 scenarios. Unit: °C

projected to show prominent increases over the LMRB, exhibiting more intense warming in the SSP5-8.5 scenario. For TXx, The most remarkable warming is predominantly projected in the Lancang River Basin. Relative to the reference period, the mid-term and long-term warming of TXx in SSP5-8.5scenario increased by around 2.5 and 5.0 °C, respectively. Regarding TNn, the most intense warming

Table 2.5 Definitions of the extreme temperature indices employed in this section

Label	Index name	Index definition	Units
TXx	Max TX	Annual maximum value of daily maximum temperature	°C
TNn	Min TN	Annual minimum value of daily minimum temperature	°C
TX90p	Warm days	Percentage of days when the daily maximum temperature is above the 90th percentile for the base period 1961–1990	%
TN90p	Warm nights	Percentage of days when the daily minimum temperature is above the 90th percentile for the base period 1961–1990	%

also occurs in the Lancang River Basin in the future scenarios, with magnitudes of around 3.5 and 8.0 °C under the SSP5-8.5 scenario during the middle and end parts of this century, exceeding the increases in TXx. A pronounced increase in warm days (TX90p) and warm nights (TN90p) is projected to increase greatly over the southern Mekong River Basin under all SSP scenarios (around 80 and 100% for SSP5-8.5, respectively) by the end of the twenty-first century. The robust projected increases of these four indices over the LMRB suggests a potential risk of intensified temperature extremes adversely affecting natural and social systems, in light of accelerated emission trajectories. Nevertheless, consistent with the changes in mean temperatures previously discussed, the indices of extreme temperatures also appear to exhibit minimal variations over time under the SSP1-2.6 scenario, reflecting the potential efficacy of anticipated climate mitigation and adaptation strategies associated with this scenario.

To identify the inter-annual variability under different scenarios, Fig. 2.31 show the temporal evolution of regional average annual temperature extremes indices over the LMRB during 1961–2099. Generally, the CMIP6 models exhibit increasing trends in annual TXx, TNn, TX90p, and TN90p throughout the twenty-first century. Across all scenarios, a more pronounced enhancement is observed in TXx relative to TNn. By twenty-first century end, the multi-model mean projected increases in TXx and TNn are, respectively, 0.01 and 0.01 °C/yr in SSP1-2.6, 0.03 and 0.03 °C/yr in SSP2-4.5, 0.05 and 0.05 °C/yr in SSP3-7.0, and 0.07 and 0.06 °C/yr in SSP5-8.5. The increasing trends of TN90p are greater than that of warm days (TX90p), likely due to amplified water vapour and radiative feedbacks at lower air temperatures. Towards the end of the twenty-first century, the warming trends for TX90p and TN90p over the Basin are 0.15 and 0.20%/yr for SSP1-2.6, 0.38 and 0.45%/yr for SSP2-4.5, 0.57 and 0.57%/yr for SSP3-7.0, and 0.69 and 0.72%/yr for SSP5-8.5.

It is noticed that the observed trend of TNn is larger than that of TXx (Figs. 2.9b and 2.11b), but the simulated future changes of TXx are higher than those of TNn (Fig. 2.13). In fact, the observed warming is much faster in TN (homogeneously) than the TX, which is similar to the observed change in global temperature as shown in IPCC AR6 (Fig. 11.2 in Chap. 11 of IPCC AR6). This is associated with a decrease in the diurnal temperature range (DTR). Various localized factors such as cloud cover,

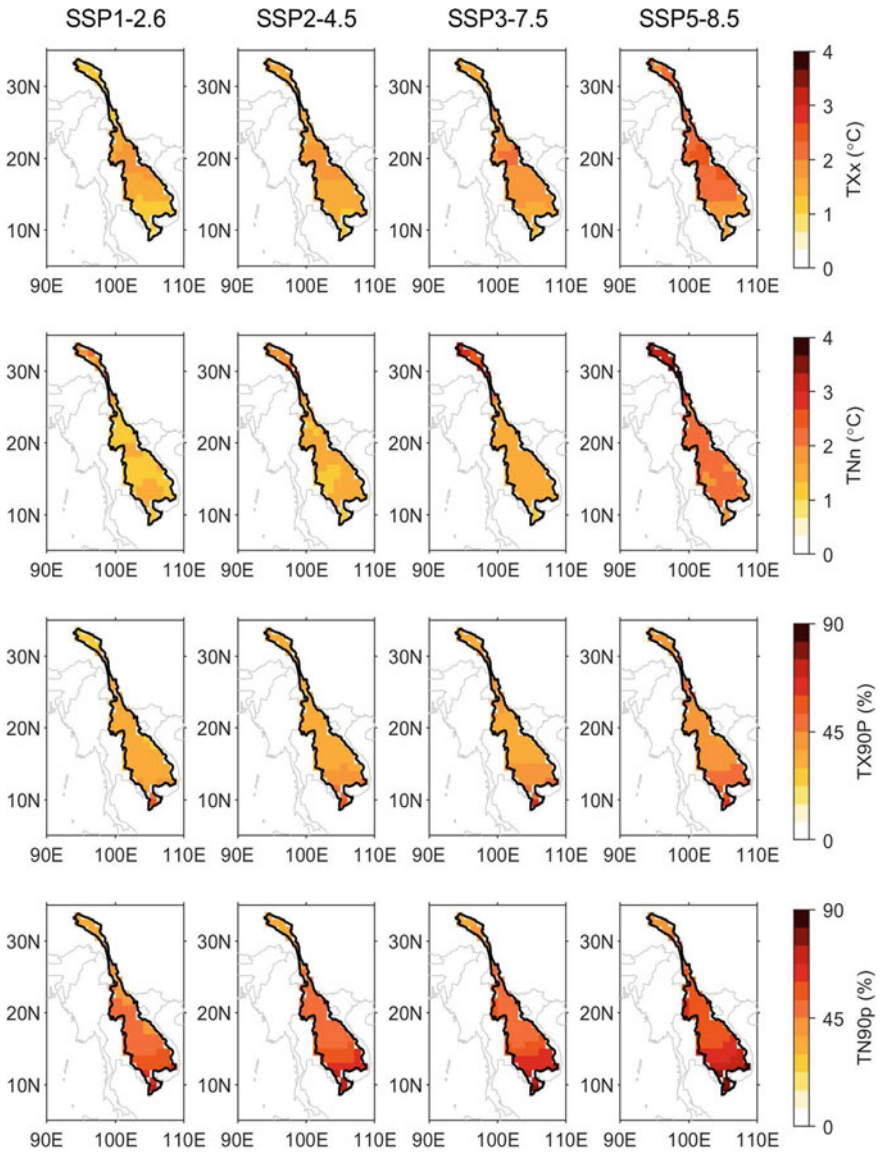

Fig. 2.29 Spatial distributions of projected changes in annual mean max TX (TXx), min TN (TNn), warm days (TX90p), and warm nights (TN90p) for the mid-term (2041–2060) period relative to the reference period 1995–2014 under the SSP1-2.6, SSP2-4.5, SSP3-7.0, and SSP5-8.5 scenarios. Note that TX90p and TN90p are displayed as absolute exceedance rates

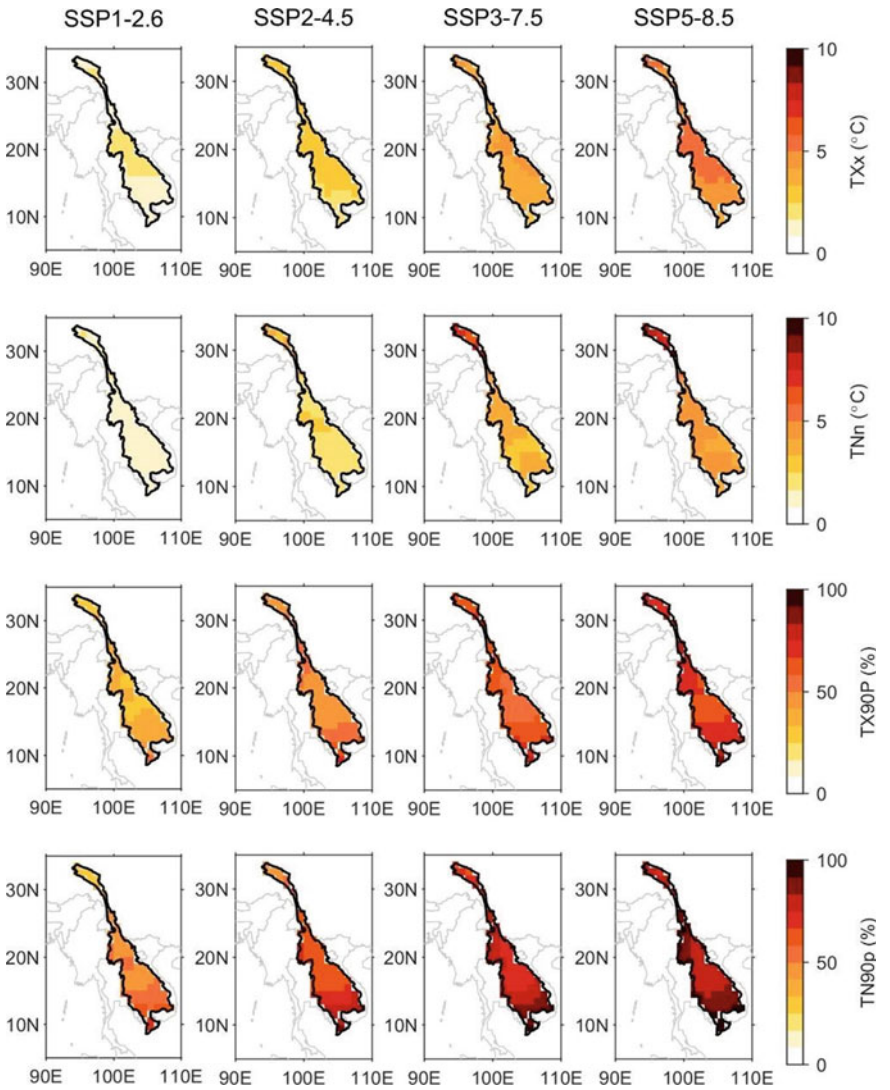

Fig. 2.30 Spatial distributions of projected changes in annual mean max TX (TXx), min TN (TNn), warm days (TX90p), and warm nights (TN90p) for the long-term (2081–2100) period relative to the reference period 1995–2014 under the SSP1-2.6, SSP2-4.5, SSP3-7.0, and SSP5-8.5 scenarios. Note that TX90p and TN90p are displayed as absolute exceedance rates

soil moisture, and precipitation significantly influence the DTR variations (Davy et al., 2017). Future projections imply that modifications in these local conditions could potentially amplify the DTR, marking a reversal from the current observed patterns.

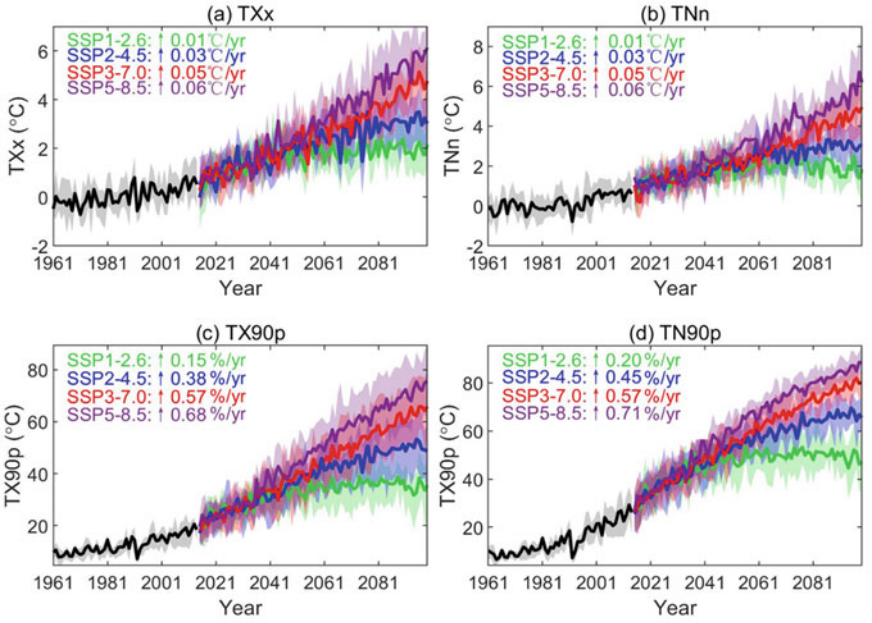

Fig. 2.31 Time series of changes in annual mean max TX (TXx), min TN (TNn), warm days (TX90p), and warm nights (TN90p) over the LMRB during 1961–2100 relative to the period 1995–2014. (Note that the time series for TX90p and TN90p are displayed as an absolute exceedance rate). The black, green, blue, red, and purple curves represent the results for the CMIP6 ensemble mean for the historical period and the SSP1-2.6, SSP2-4.5, SSP3-7.0, and SSP5-8.5 scenarios, respectively. The shaded areas are the spreads from the 25th to the 75th percentiles of the annual mean temperature extreme indices

References

Adam, J. C., & Lettenmaier, D. P. (2003). Adjustment of global gridded precipitation for systematic bias. *Journal of Geophysical Research: Atmosphers, 108*, 4257–4268. https://doi.org/10.1029/2002JD002499

Adamson, P., & Bird, J. (2010). The Mekong: A drought-prone tropical environment? *International Journal of Water Resources Development, 26*, 579–594.

Adler, R. F., Gu, G., Sapiano, M., Wang, J.-J., & Huffman, G. J. (2017). Global precipitation: Means, variations and trends during the satellite era (1979–2014). *Surveys in Geophysics, 38*, 679–699. https://doi.org/10.1007/s10712-017-9416-4

Bannister, D., Herzog, M., Graf, H.-F., Hosking, J. S., & Short, C. A. (2017). An assessment of recent and future temperature change over the Sichuan Basin, China, using CMIP5 climate models. *Journal of Climate, 30*, 6701–6722.

Calvin, K., Bond-Lamberty, B., Clarke, L., Edmonds, J., Eom, J., Hartin, C., Kim, S., Kyle, P., Link, R., Moss, R., McJeon, H., Patel, P., Smith, S., Waldhoff, S., & Wise, M. (2017). The SSP4: A world of deepening inequality. *Global Environmental Change, 42*, 284–296.

Chang, C.-P., Lei, Y., Sui, C.-H., Lin, X., & Ren, F. (2012). Tropical cyclone and extreme rainfall trends in East Asian summer monsoon since mid-20th Century. *Geophysical Research Letters*. https://doi.org/10.1029/2012GL052945

Chen, A., Chen, D., & Azorin-Molina, C. (2018). Assessing reliability of precipitation data over the Mekong River Basin: A comparison of ground-based, satellite, and reanalysis datasets. *International Journal of Climatology, 38*(11), 4314–4334.

Chen, A., Ho, C.-H., Chen, D., & Azorin-Molina, C. (2019). Tropical cyclone rainfall in the Mekong River Basin for 1983–2016. *Atmospheric Research, 226*, 66–75.

Chen, A., Emanuel, K. A., Chen, D., Lin, C., & Zhang, F. (2020a). Rising future tropical cyclone-induced extreme winds in the Mekong River Basin. *Science Bulletin, 65*, 419–424.

Chen, A., Giese, M., & Chen, D. (2020b). Flood impact on Mainland Southeast Asia between 1985 and 2018—The role of tropical cyclones. *Journal of Flood Risk Management*. https://doi.org/10.1111/jfr3.12598

Costa-Cabral, M. C., Richey, J. E., Goteti, G., Lettenmaier, D. P., Feldkötter, C., & Snidvongs, A. (2008). Landscape structure and use, climate, and water movement in the Mekong River basin. *Hydrological Processes, 22*, 1731–1746.

Dang, V. H., et al. (2020). Assessment of rainfall distributions and characteristics in coastal provinces of the Vietnamese Mekong Delta under climate change and ENSO processes. *Water-Sui, 12*, 1555.

Davy, R., Esau, I., Chernokulsky, A., Outten, S., & Zilitinkevich, S. (2017). Diurnal asymmetry to the observed global warming. *International Journal of Climatology, 37*, 79–93. https://doi.org/10.1002/joc.4688

Ding, Y., & Chan, J. (2005). The East Asian summer monsoon: An overview. *Meteorology and Atmospheric Physics, 89*, 117–142.

Dunn, R. J. H., et al. (2020). Development of an updated global land in situ-based data set of temperature and precipitation extremes: HadEX3. *Journal of Geophysical Research: Atmospheres, 125*, e2019JD032263.

Eyring, V., Bony, S., Meehl, G. A., Senior, C. A., Stevens, B., Stouffer, R. J., & Taylor, K. E. (2016). Overview of the Coupled model intercomparison project phase 6 (CMIP6) experimental design and organisation. *Geoscientific Model Development, 9*, 1937–1958.

Eyring, V., Cox, P. M., Flato, G. M., Gleckler, P. J., Abramowitz, G., Caldwell, P., Collins, W. D., Gier, B. K., Hall, A. D., Hoffman, F. M., Hurtt, G. C., Jahn, A., Jones, C. D., Klein, S. A., Krasting, J. P., Kwiatkowski, L., Lorenz, R., Maloney, E., Meehl, G. A., … Williamson, M. S. (2019). Taking climate model evaluation to the next level. *Nature Climate Change, 9*, 102–110.

Fan, H., & He, D. (2015). Temperature and precipitation variability and its effects on streamflow in the upstream regions of the Lancang-Mekong and Nu–Salween Rivers. *Journal of Hydrometeorology, 16*(5), 2248–2263.

Fan, X., & Luo, X. (2019). Precipitation and flow variations in the Lancang-Mekong River Basin and the implications of monsoon fluctuation and regional topography. *Water, 11*(10), 2086.

Fricko, O., Havlik, P., Rogelj, J., Klimont, Z., Gusti, M., Johnson, N., Kolp, P., Strubegger, M., Valin, H., Amann, M., Ermolieva, T., Forsell, N., Herrero, M., Heyes, C., Kindermann, G., Krey, V., McCollum, D. L., Obersteiner, M., Pachauri, S., … Riahi, K. (2017). The marker quantification of the shared socioeconomic pathway 2: A middle-of-the-road scenario for the 21st century. *Global Environmental Change, 42*, 251–267.

Fu, Y. H., Gao, X. J., Zhu, Y. M., & Guo, D. (2021a). Climate change projection over the Tibetan Plateau based on a set of RCM simulations. *Advances in Climate Change Research*, 313–321, https://doi.org/10.1016/j.accre.2021.01.004

Fu, Y. H., Gao, X. J., Xu, Y., & Giorgi, F. (2021b). Climate change projection over Mainland Southeast Asia and the LMRB based on a set of RegCM4 simulations. *International Journal of Climatology*, under review.

Fujimori, S., Hasegawa, T., Masui, T., Takahashi, K., Herran, D. S., Dai, H., Hijioka, Y., & Kainuma, M. (2017). SSP3: AIM implementation of shared socioeconomic pathways. *Global Environmental Change, 42*, 268–283.

Gao, X. J., Xu, Y., Zhao, Z. C., Pal, J. S., & Giorgi, F. (2006). On the role of resolution and topography in the simulation of East Asia precipitation. *Theoretical and Applied Climatology, 86*, 173–185. https://doi.org/10.1007/s00704-005-0214-4

Gao, X. J., Shi, Y., Zhang, D. F., Wu, J., Giorgi, F., Ji, Z. M., & Wang, Y. G. (2012). Uncertainties of monsoon precipitation projection over China: Results from two high resolution RCM simulations. *Climate Research, 52*, 213–226. https://doi.org/10.3354/cr01084

Gao, X. J., Wu, J., Shi, Y., et al. (2018). Future changes in thermal comfort conditions over China based on multi- RegCM4 simulations. *Atmospheric and Oceanic Science Letters 11*, 291–299. https://doi.org/10.1080/16742834.2018.1471578

Giorgi, F., Hurrell, J. W., Marinucci, M. R., & Beniston, M. (1997). Elevation dependency of the surface climate change signal: A model study. *Journal of Climate, 10*, 288–296. https://doi.org/10.1175/1520-0442(1997)010%3c0288:EDOTSC%3e2.0.CO;2

Giorgi, F., Coppola, E., Solmon, F., et al. (2012). RegCM4: Model description and preliminary tests over multiple CORDEX domains. *Climate Research 52,* 7–29. https://doi.org/10.3354/cr01018

Guo, H., Bao, A., Liu, T., Ndayisaba, F., He, D., Kurban, A., & De Maeyer, P. (2017). Meteorological drought analysis in the Lower Mekong Basin using satellite-based long-term CHIRPS product. *Sustainability-Basel, 9*, 901.

Harris, I., Jones, P. D., Osborn, T. J., & Lister, D. H. (2013), Updated high-resolution grids of monthly climatic observations—The CRU TS3.10 Dataset. *International Journal of Climatology.* https://doi.org/10.1002/joc.3711

Hasson, S., Lucarini, V., & Pascale, S. (2013). Hydrological cycle over South and Southeast Asian river basins as simulated by PCMDI/CMIP3 experiments. *Earth System Dynamics, 4*, 199–217.

Hasson, S. U., Pascale, S., Lucarini, V., & Böhner J. (2016). Seasonal cycle of precipitation over major river basins in South and Southeast Asia: A review of the CMIP5 climate models data for present climate and future climate projections. *Atmospheric Research, 180*, 42–63.

Huang, Y., Wang, F., Li, Y., & Cai, T. (2014). Multi-model ensemble simulation and projection in the climate change in the Mekong River Basin. Part I: Temperature. *Environmental Monitoring and Assessment, 186*, 7513–7523.

Irannezhad, M., Liu, J., & Chen, D. (2021). Extreme precipitation variability across the LMRB during 1952–2015 in relation to teleconnections and summer monsoons. *International Journal of Climatology*. https://doi.org/10.1002/joc.7370

Irannezhad, M., Liu, J., & Chen, D. (2020). Influential climate teleconnections for spatiotemporal precipitation variability in the Lancang-Mekong River basin from 1952 to 2015. *Journal of Geophysical Research: Atmospheres, 125*(21), e2020JD033331.

Kriegler, E., Edmonds, J., Hallegatte, S., Ebi, K. L., Kram, T., Riahi, K., Winkler, H., & van Vuuren, D. P. (2014). A new scenario framework for climate change research: The concept of shared climate policy assumptions. *Climatic Change, 122*, 401–414.

Kriegler, E., Bauer, N., Popp, A., Humpenöder, F., Leimbach, M., Strefler, J., Baumstark, L., Bodirsky, B. L., Hilaire, J., Klein, D., Mouratiadou, I., Weindl, I., Bertram, C., Dietrich, J.-P., Luderer, G., Pehl, M., Pietzcker, R., Piontek, F., Lotze-Campen, H., … Edenhofer, O. (2017). Fossil-fueled development (SSP5): An energy and resource intensive scenario for the 21st century. *Global Environmental Change, 42*, 297–315.

Lee, S. K., & Dang, T. A. (2019). Spatio-temporal variations in meteorology drought over the Mekong River Delta of Vietnam in the recent decades. *Paddy and Water Environment, 17*, 35–44.

Lee, J. Y., Marotzke, J., Bala, G., Cao, L., Corti, S., Dunne, J. P., Engelbrecht, F., Fischer, E., Fyfe, J. C., Jones, C., Maycock, A., Mutemi, J., Ndiaye, O., Panickal, S., & Zhou, T. (2021). Future global climate: Scenario based projections and near-term information. In: V. Masson-Delmotte, P. Zhai, A. Pirani, S. L. Connors, C. Péan, S. Berger, N. Caud, Y. Chen, L. Goldfarb, M. I. Gomis, M. Huang, K. Leitzell, E. Lonnoy, J. B. R. Matthews, T. K. Maycock, T. Waterfield, O. Yelekçi, R. Yu, & B. Zhou (Eds.), *Climate change 2021: The physical science basis. Contribution of Working Group I to the sixth assessment report of the intergovernmental panel on climate change*. Cambridge University Press. (in press).

Li, Q., Zeng, T., Chen, Q., et al. (2022). Spatio-temporal changes in daily extreme precipitation for the Lancang-Mekong River Basin. *Natural Hazards*. https://doi.org/10.1007/s11069-022-05569-4

Liu, S. N., & Wang, J. (2020). Study on the seasonal different characteristics of streamflow and climate factors in the LMRB. *Transactions of Atmospheric Sciences, 43*, 1031–1041. (in Chinese).

Liu, L., Bai, P., Liu, C., Tian, W., & Liang, K. (2020). Changes in extreme precipitation in the Mekong Basin. *Advances in Meteorology, 2020*, 8874869.

Liu, J., Chen, D., Mao, G., Irannezhad, M., & Pokhrel, Y. (2021). Past and future changes in climate and water resources in the LMRB: Current understanding and future research directions. *Engineering*. https://doi.org/10.1016/j.eng.2021.06.026

Ma, Z. F., Liu, J., Zhang, S. Q., Chen, W. X., & Yang, S. Q. (2013). Observed climate changes in southwest China during 1961–2010. *Advances in Climate Change Research, 4*(1), 30–40.

Mekong River Commission (MRC), 2010Mekong River Commission (MRC). (2010). State of the Basin Report 2010. Mekong River Commission. Vientiane, Lao PDR. 1728, 3248.

Moss, R. H., Edmonds, J. A., Hibbard, K. A., Manning, M. R., Rose, S. K., van Vuuren, D. P., Carter, T. R., Emori, S., Kainuma, M., Kram, T., Meehl, G. A., Mitchell, J. F., Nakicenovic, N., Riahi, K., Smith, S. J., Stouffer, R. J., Thomson, A. M., Weyant, J. P., & Wilbanks, T. J. (2010). The next generation of scenarios for climate change research and assessment. *Nature, 463*, 747–756.

O'Neill, B. C., Tebaldi, C., van Vuuren, D. P., Eyring, V., Friedlingstein, P., Hurtt, G., Knutti, R., Kriegler, E., Lamarque, J. F., Lowe, J., Meehl, G. A., Moss, R., Riahi, K., & Sanderson, B. M. (2016). The scenario model intercomparison project (ScenarioMIP) for CMIP6. *Geoscientific Model Development, 9*, 3461–3482.

Räsänen, T. A., & Kummu, M. (2013). Spatiotemporal influences of ENSO on precipitation and flood pulse in the Mekong River Basin. *Journal of Hydrology, 476*, 154–168.

Ruan, Y., Yao, Z., Wang, R., & Liu, Z. (2018). Ranking of CMIP5 GCM Skills in simulating observed precipitation over the Lower Mekong Basin. Using an improved score-based method. *Water-Sui, 10*, 1868.

Ruan, Y., Liu, Z., Wang, R., & Yao, Z. (2019). Assessing the performance of CMIP5 GCMs for Projection of future temperature change over the Lower Mekong Basin. *Atmosphere-Basel, 10*, 93.

Sooraj, K. P., Terray, P., & Mujumdar, M. (2015). Global warming and the weakening of the Asian summer monsoon circulation: Assessments from the CMIP5 models. *Climate Dynamics, 45*(1–2), 233–252.

Su, F., Duan, X., Chen, D., Hao, Z., & Cuo, L. (2013). Evaluation of the global climate models in the CMIP5 over the Tibetan Plateau. *Journal of Climate, 26*, 3187–3208.

Sun, C., Xiao, Z., Sun, J., & Yu, E. (2020). Projection of temperature change and extreme temperature events in the Lancang-Mekong River basin. *Atmospheric and Oceanic Science Letters, 13*, 16–25.

Tangang, F., Juneng, L., & Ahmad, S. (2007). Trend and interannual variability of temperature in Malaysia: 1961–2002. *Theoretical and Applied Climatology, 89*, 127–141. https://doi.org/10.1007/s00704-006-0263-3

Tapiador, F. J., Navarro, A., Moreno, R., Sánchez, J. L., & García-Ortega, E. (2020). Regional climate models: 30 years of dynamical downscaling. *Atmospheric Research, 235*, 104785.

Thirumalai, K., DiNezio, P. N., Okumura, Y., & Deser, C. (2017). Extreme temperatures in Southeast Asia caused by El Niño and worsened by global warming. *Nature Communications, 8*(1), 1–8.

Tian, F., et al. (2020). Drought characteristics of Lancang-Mekong River Basin and the impacts of reservoir regulation on streamflow. Research Report, Tsinghua University, Beijing, China, 30 pp. http://www.civil.tsinghua.edu.cn//upload/file/20200715/1594791768224016662.pdf

van Vuuren, D. P., Stehfest, E., Gernaat, D. E. H. J., Doelman, J. C., van den Berg, M., Harmsen, M., de Boer, H. S., Bouwman, L. F., Daioglou, V., Edelenbosch, O. Y., Girod, B., Kram, T., Lassaletta, L., Lucas, P. L., van Meijl, H., Müller, C., van Ruijven, B. J., van der Sluis, S., & Tabeau, A. (2017). Energy, land-use and greenhouse gas emissions trajectories under a green growth paradigm. *Global Environmental Change, 42*, 237–250.

Wang, W., Lu, H., Yang, D., et al. (2016). Modelling hydrologic processes in the Mekong River Basin using a distributed model driven by satellite precipitation and rain gauge observations. *PLoS One, 11*(3), e0152229.

Wang, W., et al. (2017) Dam Construction in LMRB could mitigate future flood risk from warming-induced intensified rainfall. *Geophysical Research Letters, 44*, 10378–310386.

Wang, K., Pu, T., Shi, X. Y., & Kong, Y. L. (2020). Impact of temperature and precipitation on runoff change in the source region of Lancang River. *Climate Change Research, 16*, 306–315. (in Chinese).

Wang, J., Tang, Q., Chen, A., Tang, Y., Xu, X., Yun, X., Mu, M., Wright, N., & Chen, D. (2022). Impacts of summer monsoons on flood characteristics in the LMRB. *Journal of Hydrology, 604*, 127256.

Wu, J., & Gao, X. J. (2013). A gridded daily observation dataset over China region and comparison with the other datasets. *Chinese Journal of Geophysics-CH, 56*, 1102–1111. (in Chinese).

Wu, D., Zhao, Y., Pei, Y. S., & Zhai, J. Q. (2011). Variation trends of temperature and precipitation in LMRB during 1980–2009. *Journal of China Institute of Water Resources and Hydropower Research, 9*, 304–312. (in Chinese).

Wu, F., Wang, X., Cai, Y., & Li, C. (2016). Spatiotemporal analysis of precipitation trends under climate change in the upper reach of Mekong River basin. *Quaternary International, 392*, 137–146.

Yang, R., Zhang, W.-K., Gui, S., Tao, Y., & Cao, J. (2019). Rainy season precipitation variation in the Mekong River basin and its relationship to the Indian and East Asian summer monsoons. *Climate Dynamics, 52*, 5691–5708.

Yasutomi, N., Hamada, A., & Yatagai, A. (2011). Development of a long-term daily gridded temperature dataset and its application to rain/snow discrimination of daily precipitation. *Global Environmental Research, 15*, 165–172.

Yatagai, A., Arakawa, O., Kamiguchi, K., Kawamoto, H., Nodzu, M. I., & Hamada, A. (2009). A 44-year daily gridded precipitation dataset for Asia based on a dense network of rain gauges. *Sola, 5*, 137–140.

Yatagai, A., Kaminguchi, K., Arakawa, O., Hamada, A., & Kitoh, A. (2012). APHRODITE: Constructing a long-term daily gridded precipitation dataset for Asia based on a dense network of rain gauges. *Bulletin of the American Meteorological Society, 93*, 1401–1415. https://doi.org/10.1175/BAMS-D-11-00122.1